Form Approved
Budget Bureau No. 22-R029

SEMI-ANNUAL
TECHNICAL REPORT

to the

AIR FORCE OFFICE OF SCIENTIFIC RESEARCH

from

Eugene Herrin

Geophysical Laboratory
Institute for the Study
of Earth and Man
Southern Methodist University

For the period ending September 1, 1974

ARPA Order: 2382
Program Code: 4F10
Name of Contractor: Southern Methodist University
Effective Date of Contract: January 16, 1974
Contract Expiration Date: July 15, 1976
Amount of Contract Dollars: $711,731
Contract Number: F 44620-73-C-0044
Principal Investigator and Phone Number: Eugene Herrin, #214-692-2760
Program Manager and Phone Number: Truman Cook, Director of Research Administration, #214-692-2031

Title of Work: Improved Methods for Detection of Long Period Rayleigh Waves and for Identification of Earthquakes and Underground Explosions

Sponsored by
Advanced Research Projects Agency
ARPA Order No. 2382

ESTIMATION OF DISPERSION CURVES FOR RAYLEIGH WAVES COMPLICATED BY MULTIPATH EFFECTS

by

George Alvin McKinley

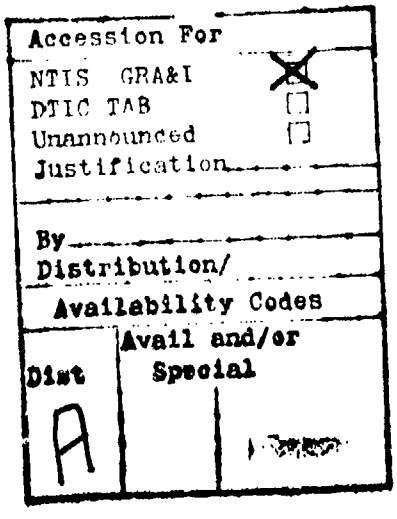

ABSTRACT

Dispersed surface waves that arrive at a seismograph by traveling other than a great-circle path, or have been delayed by reflection along the path, interfere with the first arriving great circle waves. The problem of finding the correct group velocity dispersion in the presence of such multipath interference can be simplified by the use of phase equalization filters based on assumed dispersion curves. Group velocity dispersion curves calculated using zero crossing, multiple-filter, or moving-window methods can be perturbed slightly with each perturbation yielding a different phase equalization filter. Cross-correlation of the "chirp" implied by the filter with the dispersed wave train produces a time function whose real spectrum can be computed. The process is repeated with different trial "chirps" until the integral of the real part of the spectrum is maximized. The associated dispersion curve is then considered to be a "best estimate" of the true curve. Application of the technique to synthetic seismograms has shown a resolution significantly greater than existing methods when multipath effects are present. The use of this method is demonstrated with teleseismic Rayleigh waves recorded at LASA.

TABLE OF CONTENTS

LIST OF ILLUSTRATIONS

INTRODUCTION

If Rayleigh waves propagated only in a laterally homogeneous, layered half-space the dispersion curves obtained by the calculation of periods and velocities from the peak and trough or zero crossing method (Ewing and Press, 1952; McDonald et al., 1974) or from Fourier analysis (Sato, 1955; Block and Hales, 1968; Landisman et al., 1969; Dziewonski et al., 1969) would be the true dispersion curves. However, dispersion data obtained by these techniques are almost invariably discontinuous; many show non-least time arrivals (energy refracted or reflected from lateral boundaries) which interfere with the wave that has traveled a true great circle path. The effect of superposition of multipathed signals with the primary signal is to produce a spectrum with "holes" and "buildups" at various frequencies. In addition, significant errors are introduced into the estimation of the dispersion curve. In order to obtain a correct dispersion curve for a particular travel path for either Rayleigh or Love waves, the effects of multipathing must be removed.

CHIRP FILTERING

Basic Principles

The concept of phase equilization (or chirp) filtering can be utilized in the estimation of dispersion curves for Rayleigh waves which have been complicated by multipathing. If an initial estimate of the unknown curve is made (e.g. the world-wide average for continental or oceanic paths of Oliver (1962) would suffice), a corresponding chirp wave form can be generated for this estimate by the method of McDonald et al. (1974). Dispersion curves used in this process should be continuous, monotonically increasing functions; thus the resulting chirps will be smoothly dispersed signals of constant amplitude with phase determined by the estimate of the dispersion curve.

Let c(t) be the chirp derived from an estimated dispersion curve and g(t) the recorded signal. Then

$$G(t) \star C(t) = \int_{-\infty}^{\infty} g(t)\, c(t+T)dt = H(T)$$

where H(T) is the cross-correlation function. The Fourier transform of H(T) can be written

$$G(\omega)\ C(\omega)\ \exp\ i\ \left[\phi g(\omega) - \phi c(\omega)\right]$$

or

$$G(\omega)\ C\ (\omega)\ \left\{\cos\left[\phi g(\omega) - \phi c(\omega)\right] + i\sin\left[\phi g(\omega) - \phi c(\omega)\right]\right\}.$$

Clearly the real part of the transform of H(T) will be maximized when the phase spectra of the chirp and signal are equal. In this case the amplitude spectrum $C(\omega)G(\omega)$ will be real and even. The process of maximizing the integral of the real spectrum corresponds in the time domain to maximizing the peak value of the correlation function. Assuming that no multipath interference is present, this maximization can be achieved in practice by varying the phase of the chirp until it matches that of the signal. The "pseudoautocorrelation" function (or Paf) is then defined as the particular H(T) obtained when phase equalization has been achieved. A Paf has two characteristics which set it apart from other cross-correlation functions: (1) it has the maximum peak possible for any constant amplitude assigned to the chirp, and (2) it is an even function about this peak.

The second condition results because the frequency domain equivalent of the Paf is real and even, and the transform of a real and even function is also real and even (Bracewell, 1965). A cross-correlation function other than a Paf can be expressed as a sum of its even and odd parts--a fact which accounts for its peak being smaller in magnitude.

If g(t) contains no multipaths, the dispersion curve could be determined by use of a trial and error method to equalize the phase spectra $\phi g(\omega)$ and $\phi c(\omega)$. The trial dispersion curve whose chirp maximizes the integral of the real part of the transform of the resulting cross-correlation function would be the most accurate estimate. Of course, if g(t) has no multipaths this analysis is unnecessary since the dispersion curve could be adequately determined by other means.

In the case where g(t) is the combination of multiple signals arriving at different times it can be shown that H(T) will have a series of peaks corresponding to each component of the total signal. Consider, for example, the case where g(t) is composed of a true great circle path signal and one multipathed arrival delayed by a time t_0.

Then

$g(t) = g_1(t) + Ag_2(t-t_0)$ where A is an amplitude factor. The correlation operation now becomes

$$H(T) = \int g(t)\, c(t+T)dt = \int \left[g_1(t) + Ag_2(t-t_0) \right] c(t+T)dt$$

$$= \int g_1(t)\, c\, (t+T)dt + A \int g_2(t-t_0)c(t+T)dt = H_1(t) + AH_2(t-t_0).$$

If the dispersion characteristics of $g_1(t)$ and $g_2(t)$ are similar, as is often the case when their travel paths are nearly the same, the second peak will be a replica of the first only delayed in time by t_0 and modified in amplitude by A.

Theoretically, H(T) endures from $-\infty$ to $+\infty$. In practice, for band limited data (15-70 sec periods, for example), the energy is nearly all contained in $\pm$ 100 sec from the peak. A 200 sec separation in the arrivals times of different signals would therefore result in noninterfering peaks and would allow the true dispersion curve to be obtained by maximizing the real part of the transform of the first peak. As time separation decreases between the primary and the

multipathed arrivals, the peaks will begin to interfere with each other and resolution will be lost. Empirically the minimum time separation for which this method yields accurate results will be shown to be less than 50 sec for data containing periods up to 70.

Examples Using Synthetic Signals

The relations just discussed can be illustrated empirically by the use of synthetic signals. Since paths from Central Asia to the United States are of special interest, a signal with dispersion characteristic of such a path was chosen (propagation distance approximately=12,000 kms). This signal (Figure 1) has a constant amplitude and a smoothly varying dispersion curve shown in Figure 2. This dispersion curve (referred to as #1) was fixed at its long period end (3.925 kms/sec at 75.5 sec) and rotated about that point. New curves were manufactured with velocity increments of .01 km/sec at a period of 17 sec. Six additional synthetic curves formed in this way are labeled #2,4,6 on the low velocity side of #1, and 3,5,7 on the high side. A chirp wave form was derived from each of these seven curves using the method of McDonald et al (1974). Each chirp was then cross-correlated with the synthetic signal to obtain seven correlation functions

with correponding numbers. Correlation functions 1, 2, and 3 are shown in Figures 3-5. Since #1 is a true autocorrelation function it displays the characteristic of eveness about the peak and has the highest peak magnitude for any of the seven correlations. See the first half of Table 1, where the magnitude of the peak for #1 was arbitrarily assigned the value of 1.

It may also be noted that correlations 2 and 3 are mirror images of each other about the peak. This characteristic results from the development of a small odd portion in each of these time series. Because chirps 2-7 have phase spectra unequal to the signal phase, the imaginary part of the transform does not vanish for these correlations as it does for #1.

The real and imaginary parts of the transform of each of the correlation functions were computed placing the maximum value of the main peak at zero time and centering a 200 sec window on this peak, then using the method of Filon (1929) for discrete transforms. The real part was integrated over the known bandwidth (72-18 sec periods) for each correlation function. These results are listed in Table 1 along with the peak magnitudes, and are shown graphically in Figure 6. For this particular

signal it is clear that the true dispersion curve could be determined from either correlation function peak magnitude or from the integrated real part of the transformed correlation functions. These criteria are nearly equivalent in sensitivity.

An application of the technique was then illustrated using a synthetic signal with a simulated multipath (Figure 7). This signal was created by delaying the first synthetic signal by 50 sec, dividing its amplitude by 2, zeroing the first 100 samples, and adding the delayed portion to the original signal. The true dispersion curve of this multipathed signal is then the same as that for the undisturbed signal. The same seven filters were then applied to the new signal. Correlations 1, 2, and 3 (Figures 8-10) show both a main peak and a smaller one delayed 50 sec, the exact time shift of the multipathed energy. The eveness of #1 has been only slightly disturbed out to the point of the second peak. An examination of the sensitivity (Table 1, second part, and Figure 6) for this signal shows nearly the same results as were obtained from the undisturbed signal. Thus the theory has been verified in these synthetic examples; it has been shown that the true dispersion curve is indeed attainable in the presence of multipathing.

APPLICATION TO SEISMIC DATA

The Large Aperture Seismic Array (LASA) is located near Billings, Montana. It consists of 21 subarrays for detection of high frequency seismic energy (pattern shown in Figure 11). All of these stations except those of the B ring include long period seismometers which record Rayleigh and Love waves. The response curve for long period data is shown in Figure 12. It should be noted that all LASA seismograms shown here are the raw data. No correction has been made for instrument response nor has there been any prefiltering of these signals.

The size of this array can cause serious problems in the estimation of dispersion curves because multi-pathed signals often create different effects at sensors separated by more than a few tens of kilometers. As a result it may appear that each site has its own particular dispersion curve even when this is not the case. For example, E2 is only 70 kms east of A0, thus if Rayleigh waves from an Asian earthquake with epicenter 10,000 kms directly north of the array are recorded at both sites, similar waveforms would be expected. Figures 13 and 14

show the vertical channel data recorded at A0 and E2 from such an earthquake (epicenter in Tadzhik, USSR). An examination of these two signals reveals little difference in the long period Rayleigh waves; however, at periods of approximately 25 sec and less the seismograms are quite different. A comparison of the recordings at F1 (Figure 15) and F3 (Figure 16) from this same earthquake also show variations from the A0 signal. Either structural differences across LASA or the very small differences in travel path have caused various multipathed signals to interfere differently with the first arriving, fundamental mode Rayleigh wave. Both the amplitude and phase have been distorted. Further evidence that multipathed energy is present can be seen from Figures 17 and 18, where the same event is shown as recorded at D3. Figure 17 is the radial component of motion at D3 and Figure 18 is the transverse. Since a Rayleigh wave has no transverse motion and Love waves would have arrived much sooner due to their faster velocity, the signal which appears in Figure 18 must have traveled other than a great circle path.

For the Tadzhik earthquake, the signals recorded at A0, C3, C4, D1, D2, D3, and D4 are very similar in

waveform and could be beam-summed to give a good increase in signal to noise ratio. However, recordings at the E and F sites which constitute the outer rings at LASA show significant effects of the multipathing problem which would seriously degrade the beam-sum.

The first step in determining a dispersion curve for the path from Tadzhik to LASA was to obtain an initial estimate of the curve. Figure 19 is a display of the A0 group velocity data computed from zero crossings. The scatter is typical of real signals and increases the difficulty in choosing a trial curve. A trial line was drawn through the data as a starting point (broken line in Figure 19).

Dispersion is clearly present in the period range of 42 - 16 sec and visibly extends to 50 and 12 for some sensors in the array. It was determined that all trial curves should range at least to 70 sec so that no hidden long period arrivals would be missed. The lower limit was set at 12 sec. A chirp filter was generated from the first trial curve and applied to the A0 signal. The resulting correlation function was then transformed using the Filon method with a 200 sec window centered on the maximum positive peak, and the real spectrum was examined and integrated over the period range of 42-16 sec.

The trial dispersion curve was perturbed at the long period end; i.e., only the 50-70 sec portion was changed. The same procedure for generating a chirp, correlating, windowing and transforming the correlation function was repeated for the new curve. The real spectra resulting from these two attempts were then compared. The curve producing the largest integrated real spectrum was determined the more accurate estimate. Continuing this technique with numerous other trial perturbations the long period end of the curve was established. The values of 3.8 kms/sec at 70 sec to 3.75 at 50 were determined best in that range. These results are in very close agreement with the findings of Oliver (1962) for continental Rayleigh waves.

Having determined the first section of the dispersion curve, perturbations were continued on successively shorter period portions until an accurate estimate was found for the entire curve. The belief in the correctness of this result is reinforced by the even property displayed in this correlation function about its peak (see Figure 20). The final curve is labeled 7B and is plotted beside the first estimate in Figure 19.

A sensitivity diagram was constructed similar to those for the synthetic signals shown earlier. With the long period end fixed the rest of the curve was rotated to obtain increments of velocity deviation at the short period end. A set of seven new curves was created for comparison with 7B. The results of integrated real spectra of the correlation function transforms are listed in Table 2 along with correlation peak magnitudes obtained from these curves. For curves of faster velocity the sensitivity for this signal is similar to that found in the synthetic signals, i.e. relative magnitudes drop as the velocity deviation is increased at the short period end. For the slower velocity curves, however, a secondary maximum exists below the correct curve. At a short period deviation of -.03 km/sec the relative magnitude rises to .93 after an initial drop to .85. This phenomenom can most likely be explained by noting that as the curve is rotated from its correct value in Figure 19 it first goes through a space where little dispersion data exists; as rotation is continued, a cluster of low velocity points is encountered which increases the correlation function peak magnitude. Having passed this area the magnitudes fall once again. See Figure 21.

Using 7B as a starting point, the dispersion curve was then determined for other sensors in the LASA array. It was found that 7B was also the most accurate estimate for all of the C and D sites as well as E1, E3, and F1. A slightly different dispersion curve (labeled 17B) was found for E2, F2, and F3 and a third variation of 7B (18B) was judged the best estimate for E4 and F4.

The three curves 7B, 17B, and 18B are very similar. The only differences occur in the period range 29-34 sec. These variations are magnified for comparison in Figure 22. A complete list of the integrated real parts of the transformed correlation functions are given in Table 3 for these three curves applied over the entire array. A geographical relationship between the sites and their corresponding dispersion curves is shown in Figure 23.

One of the secondary goals of this study was to make use of the dispersion curves determined from this technique by creating a chirp filter which would be useful in amplifying signal to noise ratio for small magnitude events near Tadzhik. It is suggested that any of these curves-- 7B, 17B, or 18B --should give a useful filter for this purpose.

This idea was tested using a small magnitude earthquake whose epicenter was located approximately 1400 kms northeast of the Tadzhik event. The signal in Figure 24 is barely recognizable on the A0 vertical channel. Figure 25 is the resulting correlation function with filter 18B applied to the signal. The increase in signal to noise ratio is apparent. Both the least time arrival and a multipath or after shock delayed 140 sec are now clearly visible.

The one difficulty encountered by this method in its present form is the amount of labor required in comparing all the trial curves brought about by the tremendous number of perturbations possible for any initial estimate. An automated system of curve variation from a preliminary estimate is needed. One way of satisfying this requirement is therefore suggested. If the initial curve is modified to a time function dependent on frequency with a fixed intercept on the time axis, it would then be possible to compute the coefficients of a fifth or sixth order polynomial which would closely approximate the curve. Let $U(f) = a+bf+cf^2+df^3+...$ then the velocity intercept (=a) could be fixed while the

initial slope (b) and the coefficient which determines the inflection point (c) would be varied slightly--enough to perturb the high frequency end of the curve through a range of ± .03 or .04 kms/sec. It is possible that a set of curves generated in this manner could have their chirps and signal correlations examined quickly and efficiently by a computer which would then search for the largest peak magnitude among the correlations and thus determine the best curve in one complete operation.

CONCLUSIONS

It has been clearly demonstrated that multipathing causes distortions in both the amplitude and phase of dispersed wavetrains. The technique proposed here for determining dispersion curves has been shown through the use of synthetic signals to give nearly identical results for both undisturbed and multipathed data. In both cases the trial curves when fixed at the long period end, could be used to determine the correct curve to within .01 km/sec deviation at the short period end. Also, evidence indicates that these results were duplicated when the method was applied to LASA Rayleigh waves in the actual determination of an unknown dispersion curve.

As demonstrated, the comparative accuracy of this technique far exceeds that expected from other methods when multipathed interference is present.

ACKNOWLEDGEMENTS

My sincere thanks go to Dr. Eugene Herrin whose idea originally launched this study, and for his suggestions and critique of the paper. Also, the author is extremely grateful to Dr. Tom Goforth who was an almost daily consultant during this research.

Funds for this project were provided by the Advanced Research Projects Agency under contract F44620-73-C-0044 P00005 monitored by the Air Force Office of Scientific Research.

TABLES

Table 1

Relative magnitudes of correlation functions for undisturbed synthetic signal

Filter	Short Period Deviation	Max. Peak	Real Integral
1	0 km/sec	1.0	1.0
2	-.01	.951	.955
3	+.01	.939	.942
4	-.02	.833	.838
5	+.02	.831	.824
6	-.03	.674	.673
7	+.03	.653	.651

Relative magnitudes of correlation functions for multipathed synthetic signal

Filter	Short Period Deviation	Max. Peak	Real Integral
1	0 km/sec	1.0	1.0
2	-.01	.955	.963
3	+.01	.950	.952
4	-.02	.852	.857
5	+.02	.835	.840
6	-.03	.724	.680
7	+.03	.699	.700

Table 2

Relative magnitudes of correlation functions for A0 Tadzhik signal

Short Period Dev. from Curve 7B		Max. Peak	Real Integral
0	km/sec	1.0	1.0
-.01		.846	.847
+.01		.826	.809
-.02		.910	.911
+.02		.825	.809
-.03		.930	.928
+.03		.778	.726
-.05		.886	.880

TABLE 3

REAL INTEGRAL OF CORRELATION FUNCTION FOR TADZHIK EARTHQUA
OF 17 MARCH 1972 9-17-10.

SITE	FILTER	INTEGRAL (E05 UNITS)
A0	7B	1.57
A0	17B	1.26
A0	18B	1.08
C3	7B	1.51
C3	17B	1.32
C3	18B	1.26
C4	7B	1.61
C4	17B	1.32
C4	18B	1.27
D1	7B	1.82
D1	17B	1.68
D1	18B	1.41
D2	7B	1.48
D2	17B	1.13
D2	18B	1.24
D3	7B	2.66
D3	17B	1.17
D3	18B	1.35
D4	7B	1.44
D4	17B	1.14
D4	18B	1.08
E1	7B	1.19
E1	17B	1.14
E1	18B	.99
E2	7B	1.41
E2	17B	1.54
E2	18B	1.49
E3	7B	1.73
E3	17B	1.48
E3	18B	1.46
E4	7B	1.06
E4	17B	1.16
E4	18B	1.22
F1	7B	.80
F1	17B	.72
F1	18B	.71
F2	7B	.60
F2	17B	.63
F2	18B	.66
F3	7B	1.34
F3	17B	1.43
F3	18B	1.39
F4	7B	1.29
F4	17B	1.36
F4	18B	1.38

FIGURES

FIGURE CAPTIONS

Figure	Caption
1	Synthetic signal.
2	Dispersion curve (#1) of synthetic signal shown in Figure 1.
3	Correlation function of synthetic signal with chirp 1. (true autocorrelation)
4	Correlation function of synthetic signal with chirp 2.
5	Correlation function of synthetic signal with chirp 3.
6	Sensitivity plot. Relative magnitudes of the correlation function peaks and the real spectral integrals for the seven chirps applied to (1) the undisturbed synthetic signal and (2) the multipathed synthetic signal.
7	Multipathed signal. The synthetic signal had its first 100 seconds zeroed; it was then shifted 50 seconds and added at half amplitude to the original signal.
8	Correlation function of multipathed signal with chirp 1.
9	Correlation function of multipathed signal with chirp 2.
10	Correlation function of multipathed signal with chirp 3.
11	LASA array map.
12	LASA long period response curve.

Figure	Caption
13	Tadzhik earthquake--A0 vertical channel.
14	Tadzhik earthquake--E2 vertical channel.
15	Tadzhik earthquake--F1 vertical channel.
16	Tadzhik earthquake--F3 vertical channel.
17	Tadzhik earthquake--D3 radial channel.
18	Tadzhik earthquake--D3 transverse channel.
19	A0 Tadzhik group velocity plot. The data points are computed from zero crossings of the signal. Curve 7B shows its relation to the dispersion data.
20	Cross correlation function of A0 Tadzhik vertical signal and chirp 7B.
21	Sensitivity plot. Relative magnitudes of correlation function peaks.
22	Curves 7B, 17B, and 18B. The differences between these curves has been accentuated by the large scale plot.
23	Sensitivity plot. Relative magnitudes of the correlation function peaks and the real spectral integrals for the eight chirps applied to the A0 Tadzhik vertical signal.
24	A0 vertical channel for an earthquake approximately 1400 kms northeast of the Tadzhik event.
25	Correlation function of event from Figure 25 with filter 18B applied.

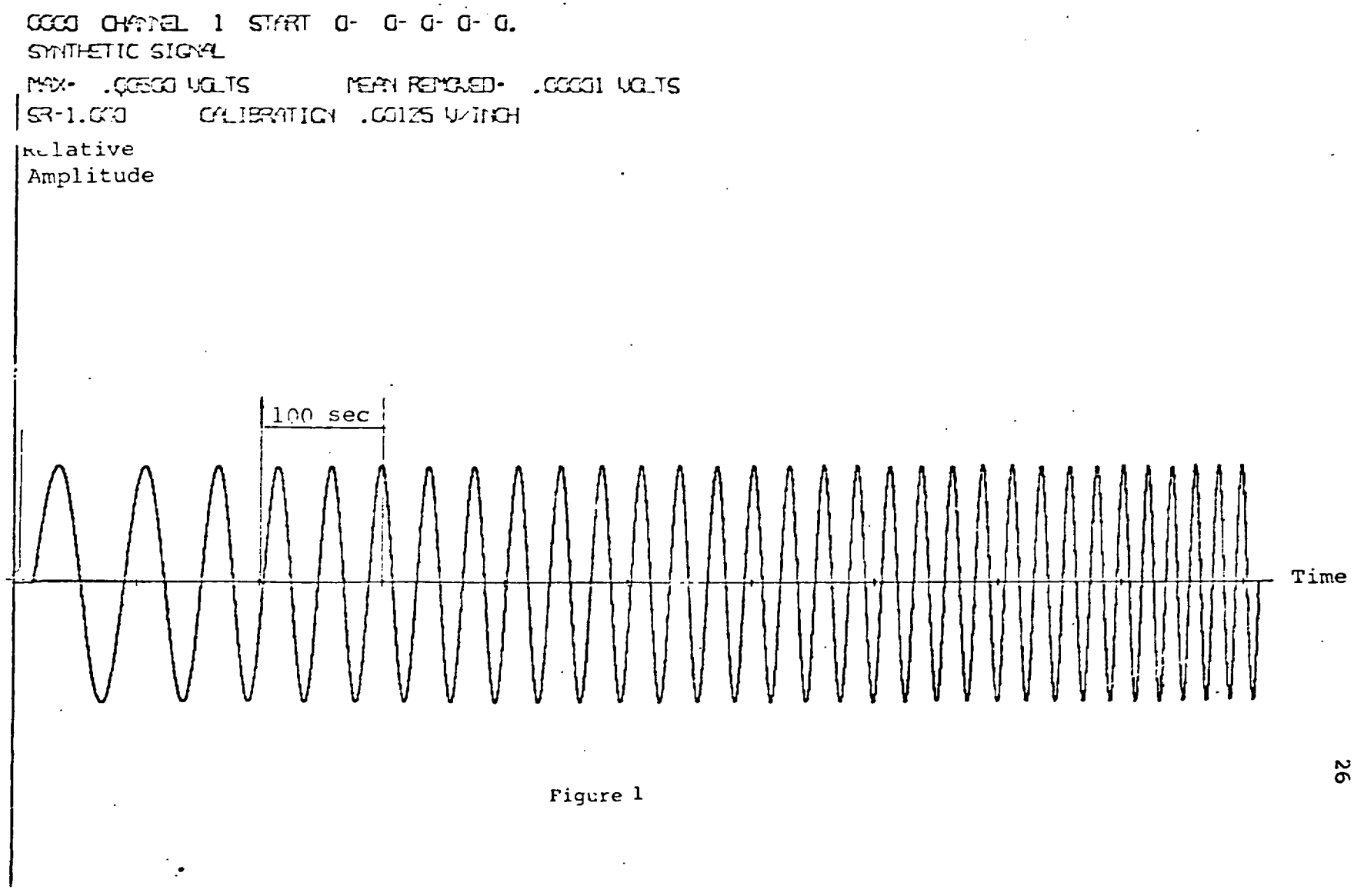
CCCC CHANNEL 1 START C- C- C- C- C.
SYNTHETIC SIGNAL
MAX- .CC550 VOLTS MEAN REMOVED- .CCCC1 VOLTS
SR-1.CC0 CALIBRATION .CC125 V/INCH
Relative
Amplitude
100 sec
Time

Figure 1

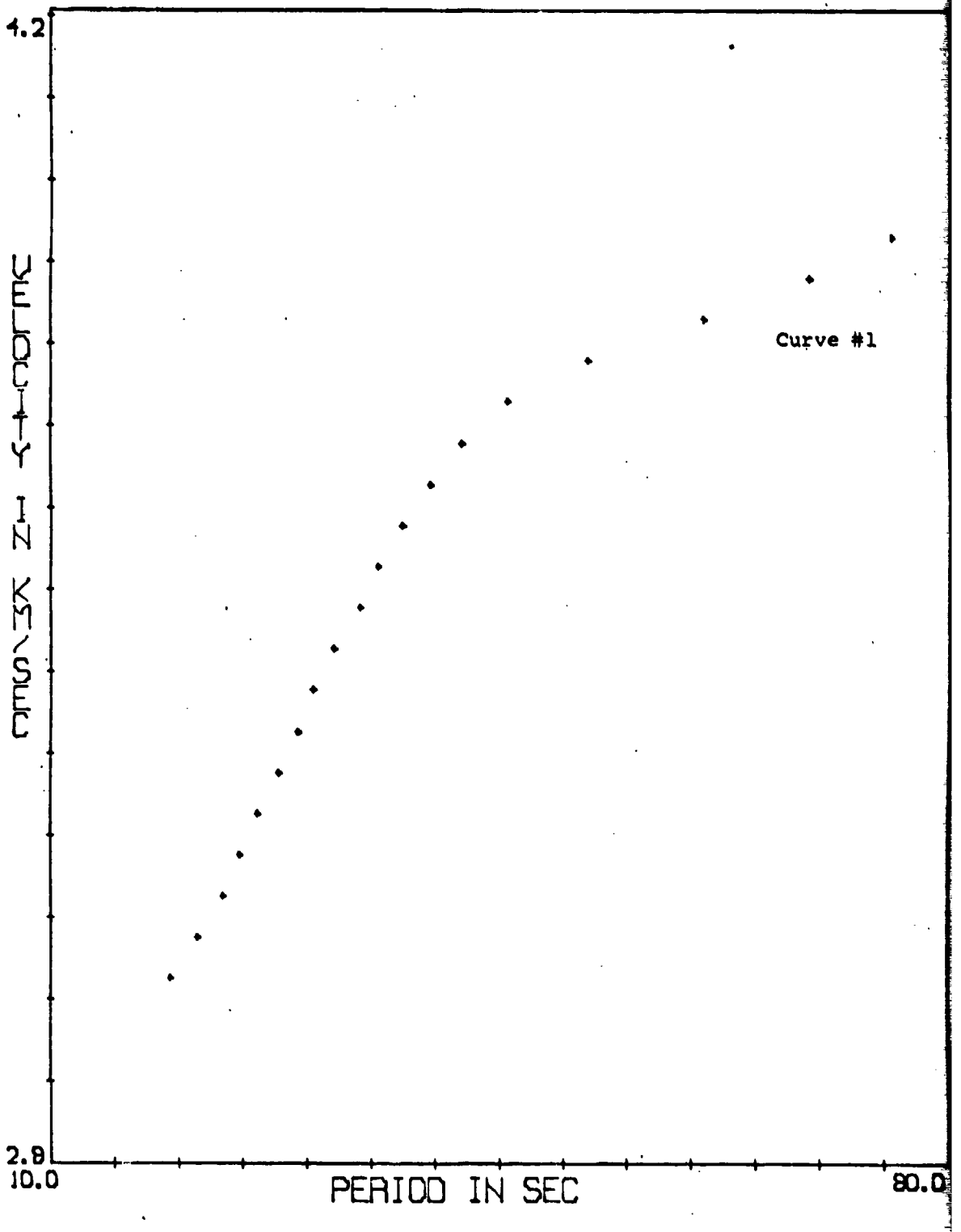

Figure 2

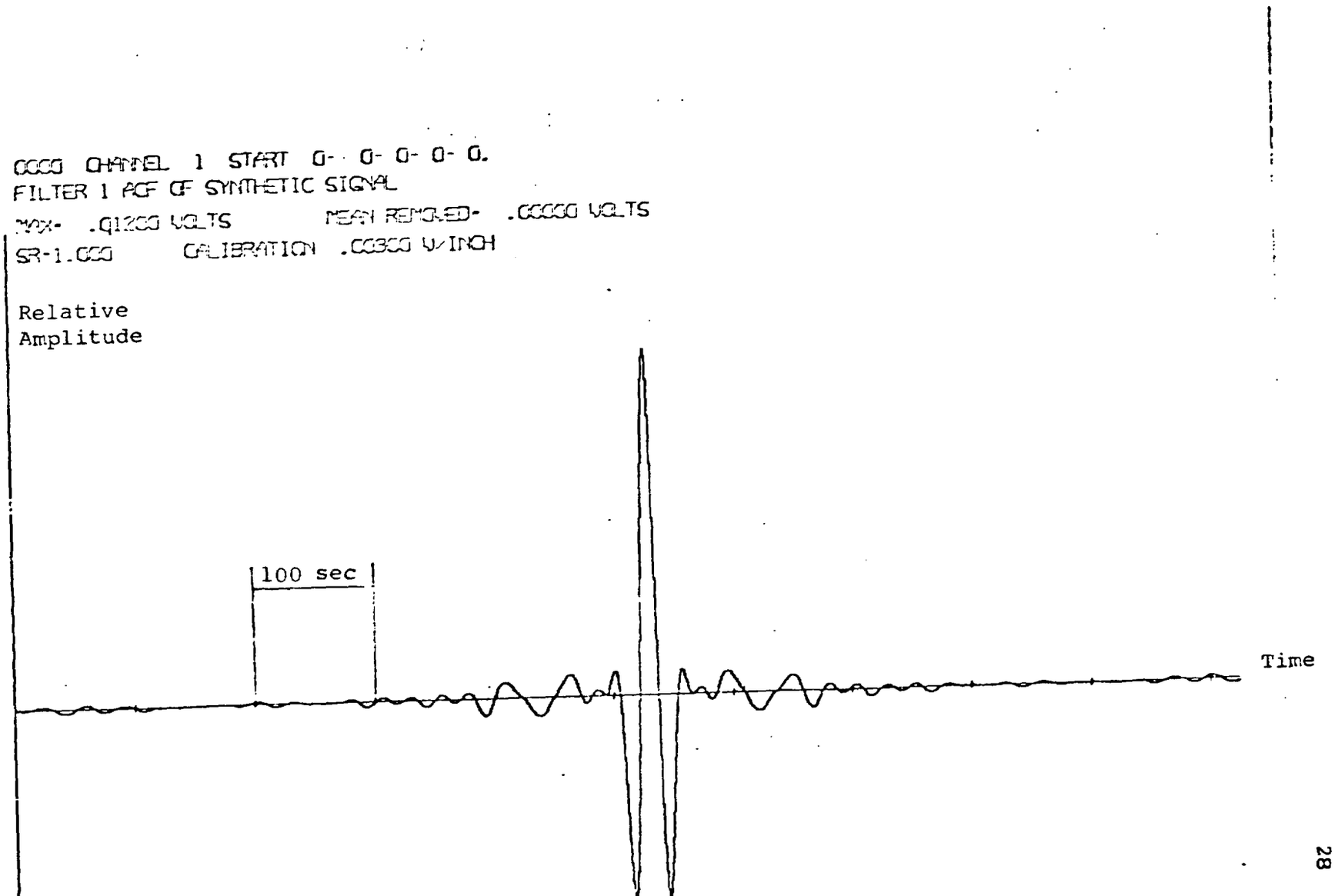
0000 CHANNEL 1 START 0- 0- 0- 0- 0.
FILTER 1 ACF OF SYNTHETIC SIGNAL
MAX- .01200 VOLTS MEAN REMOVED- .00000 VOLTS
SR-1.000 CALIBRATION .00300 V/INCH
Relative
Amplitude
100 sec
Time

Figure 3

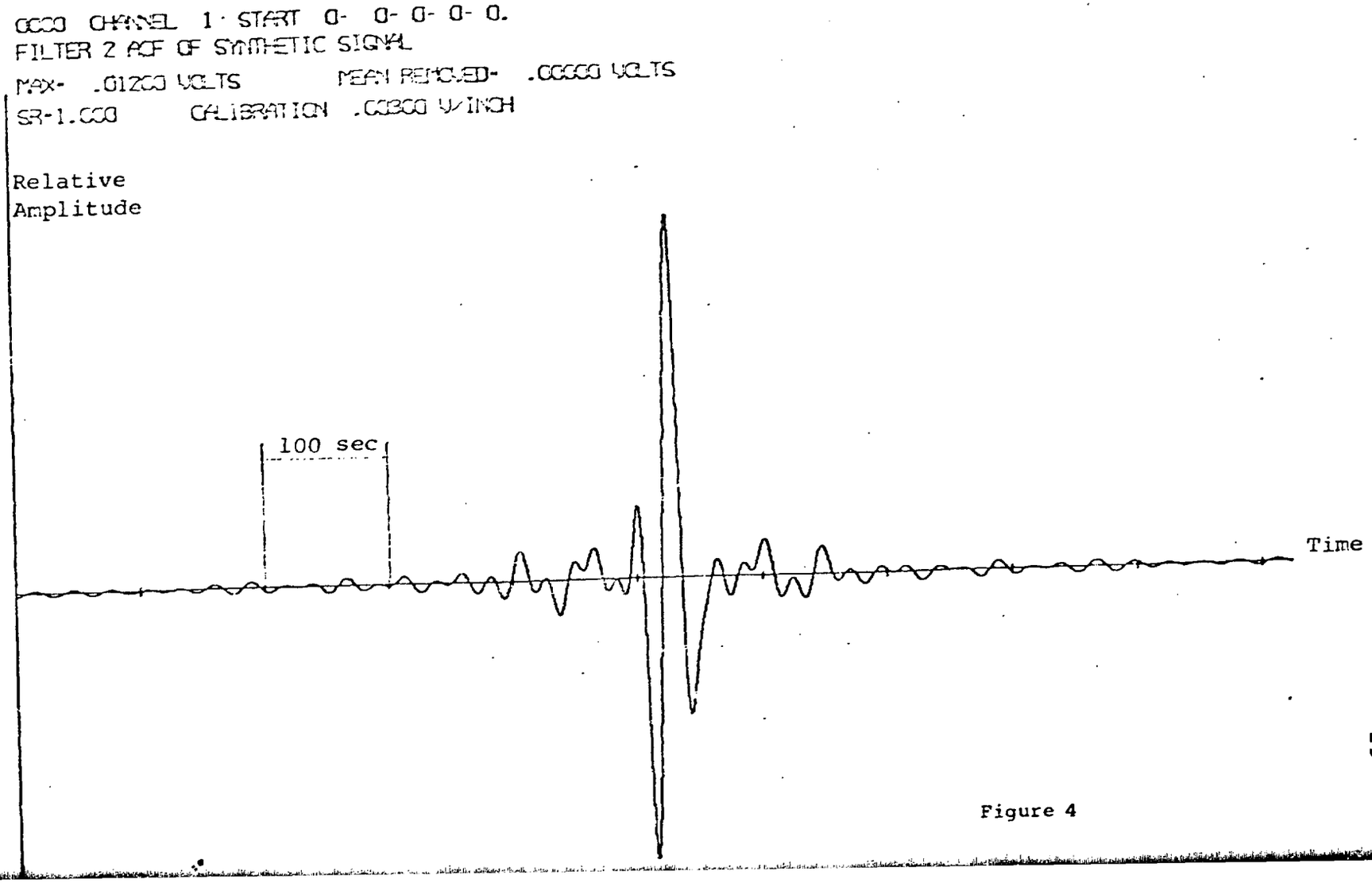
0000 CHANNEL 1 START 0- 0- 0- 0- 0.
FILTER 2 ACF OF SYNTHETIC SIGNAL
MAX- .01200 VOLTS MEAN REMOVED- .00000 VOLTS
SR-1.000 CALIBRATION .00300 V/INCH
Relative
Amplitude
100 sec
Time

Figure 4

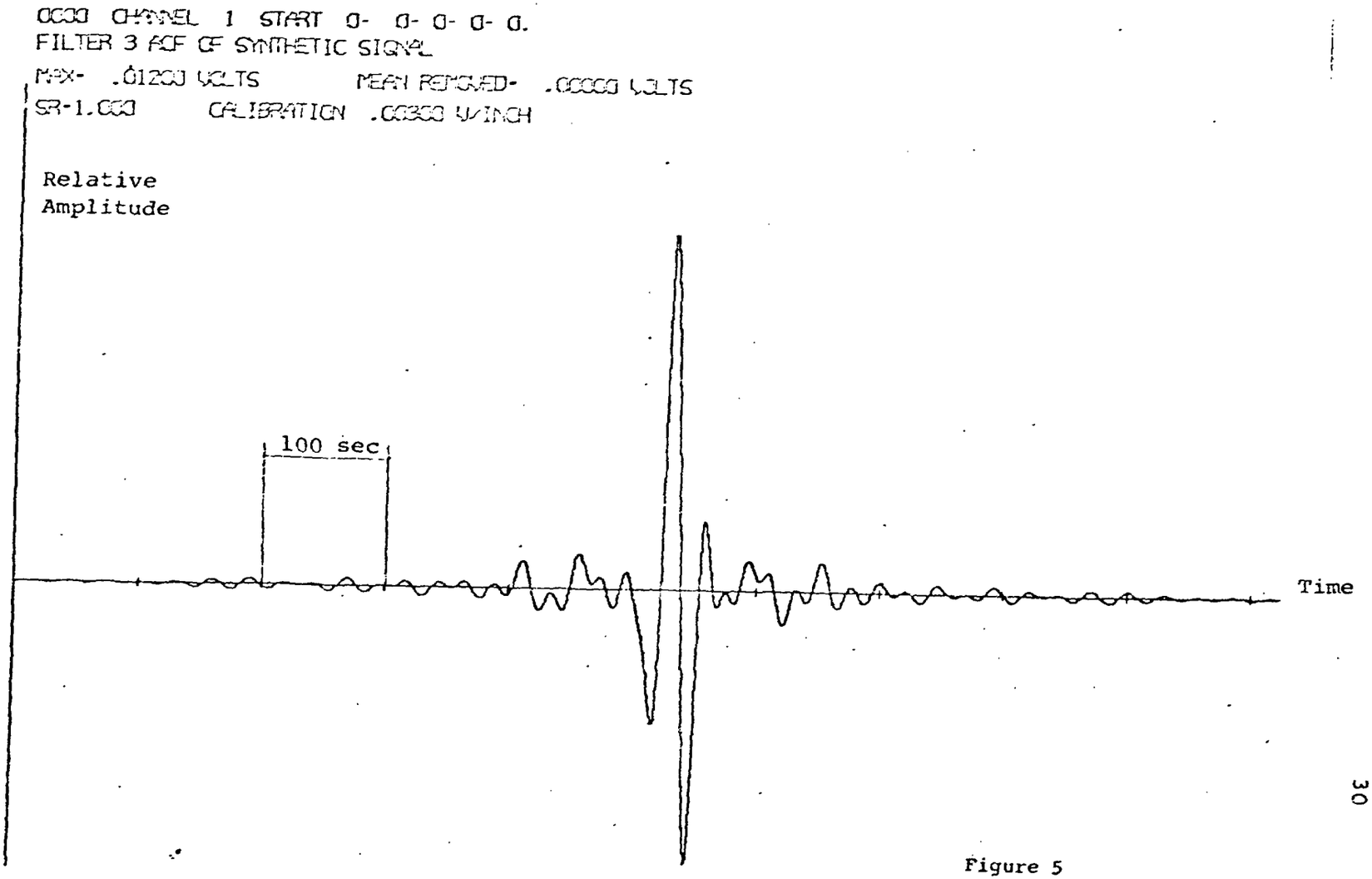
0000 CHANNEL 1 START 0- 0- 0- 0- 0.
FILTER 3 ACF OF SYNTHETIC SIGNAL
MAX- .01200 VOLTS MEAN REMOVED- .00000 VOLTS
SR-1.000 CALIBRATION .00300 V/INCH
Relative
Amplitude
100 sec
Time

Figure 5

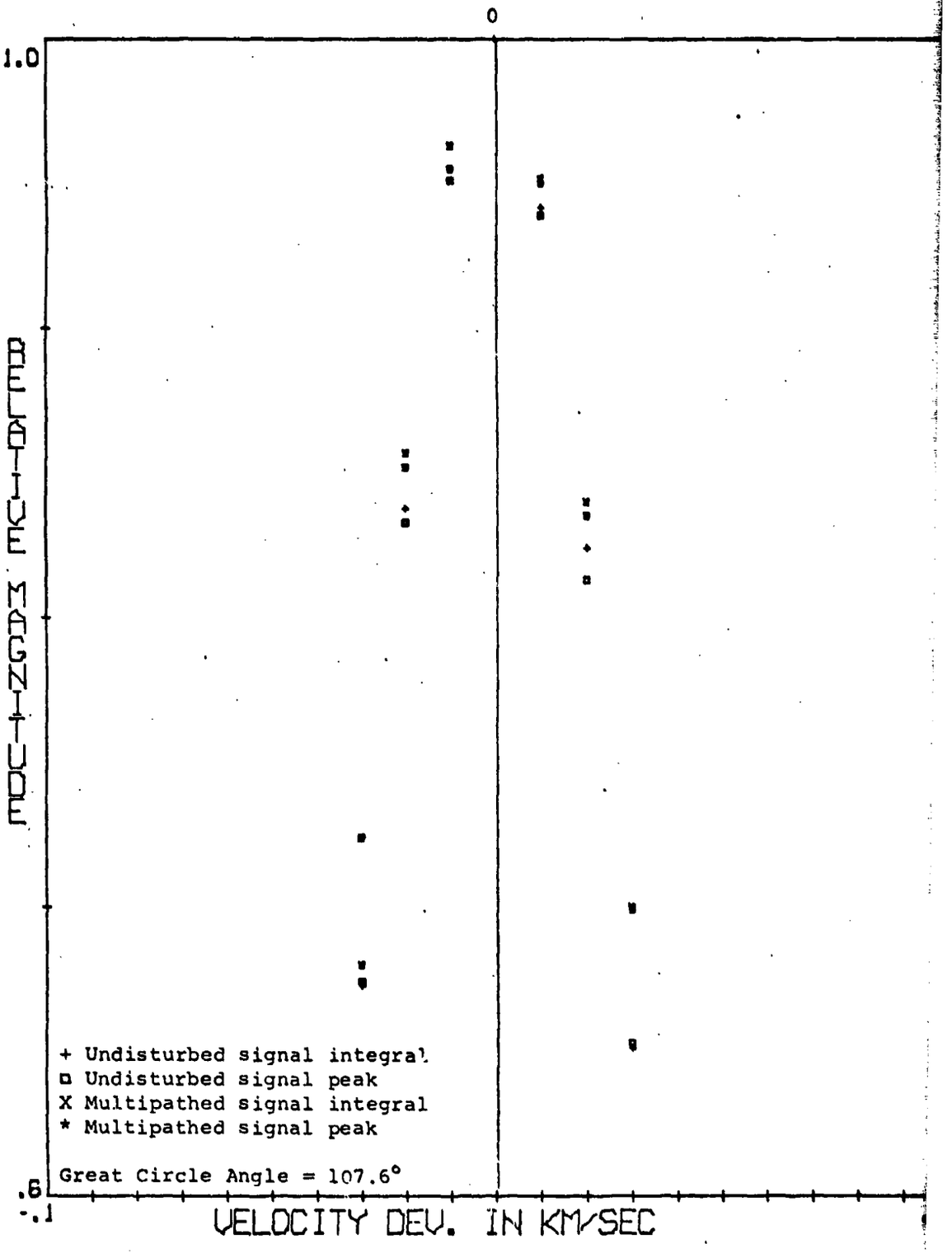
0
1.0
.6
-.1
RELATIVE SIGNAL STRENGTH
+ Undisturbed signal integral
□ Undisturbed signal peak
X Multipathed signal integral
* Multipathed signal peak
Great Circle Angle = 107.6°
VELOCITY DEV. IN KM/SEC

Figure 6

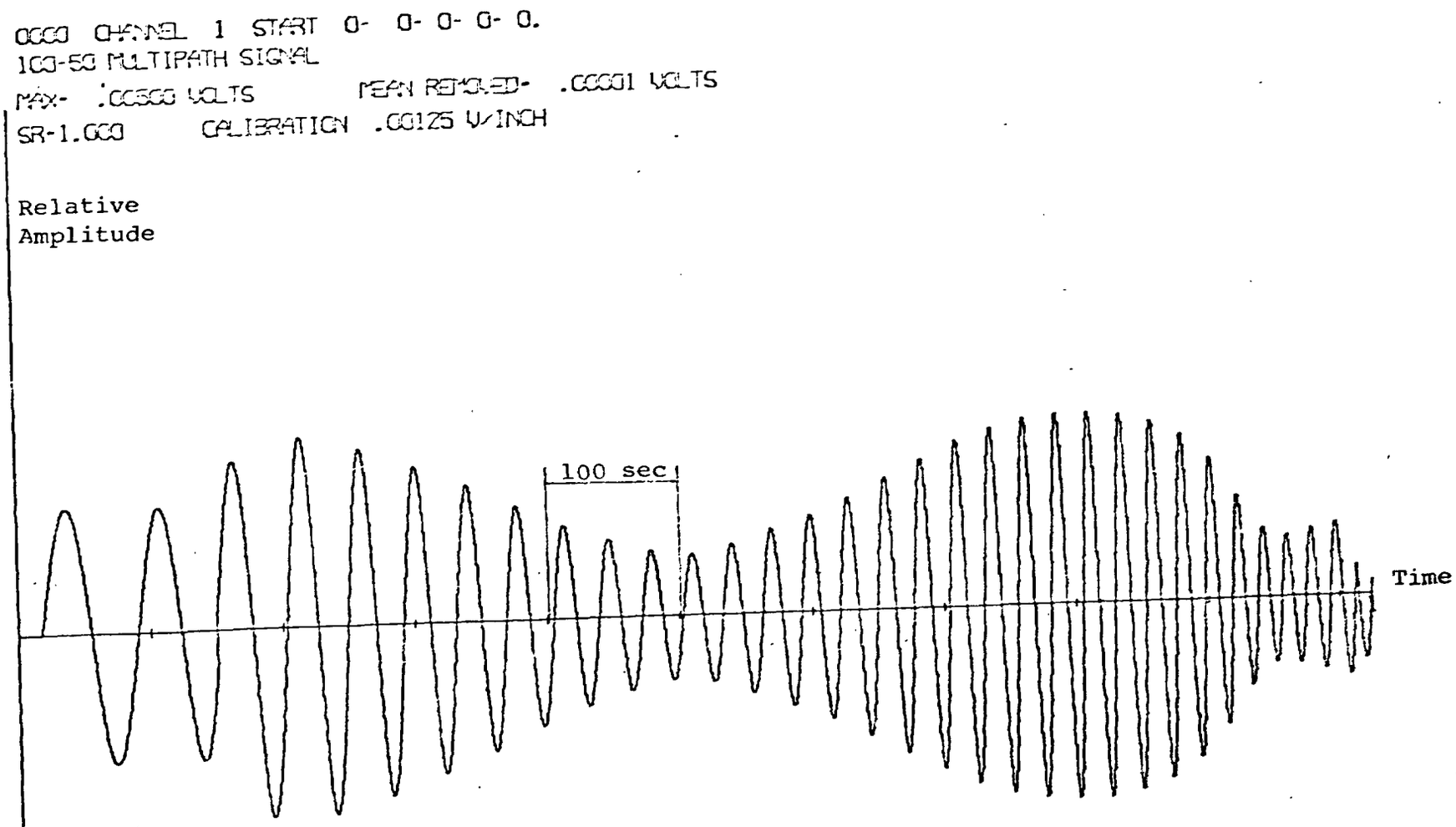
0000 CHANNEL 1 START 0- 0- 0- 0- 0.
100-50 MULTIPATH SIGNAL
MAX- .00500 VOLTS MEAN REMOVED- .00001 VOLTS
SR-1.000 CALIBRATION .00125 V/INCH
Relative
Amplitude
100 sec
Time

Figure 7

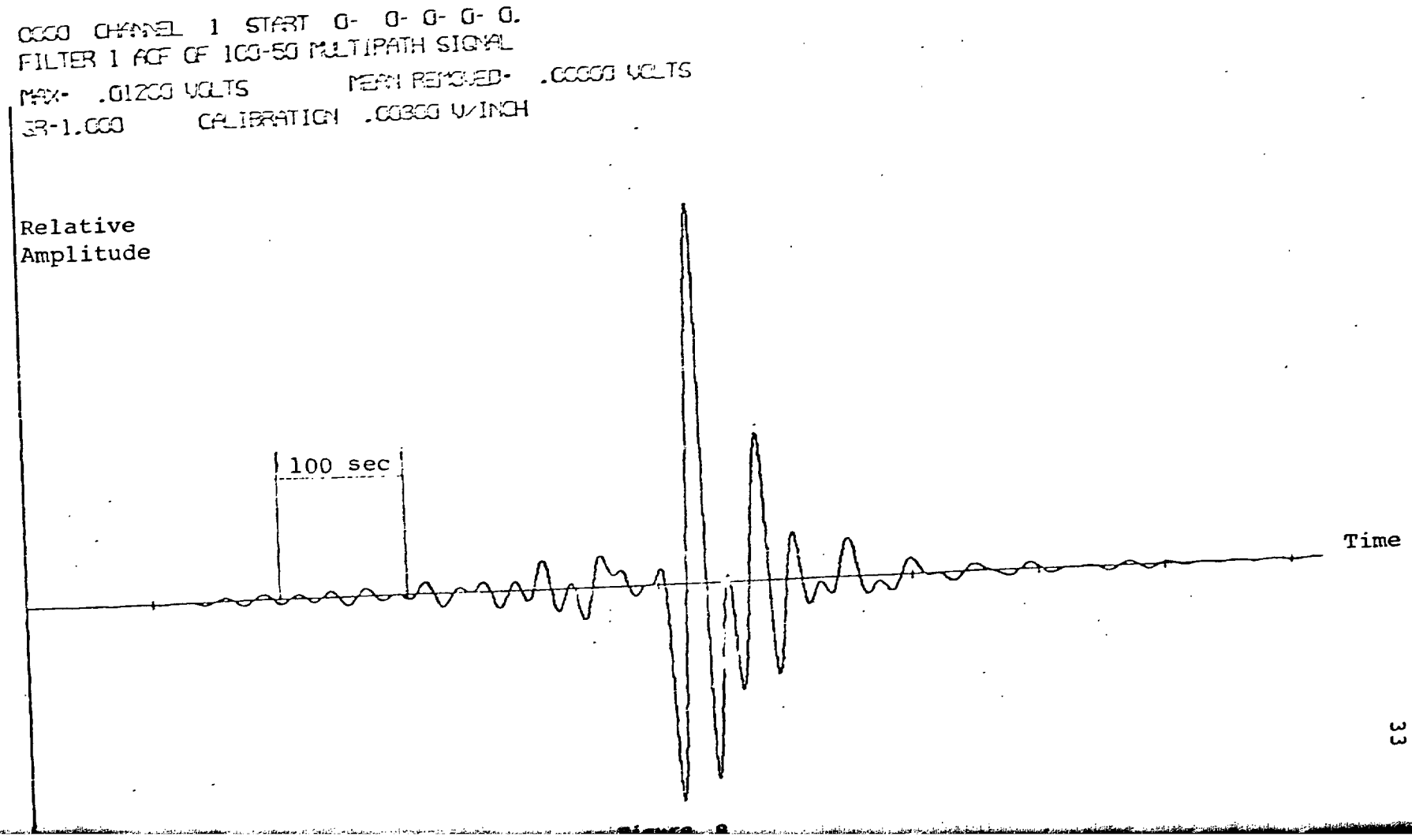
0000 CHANNEL 1 START 0- 0- 0- 0- 0.
FILTER 1 ACF OF 100-50 MULTIPATH SIGNAL
MAX- .01200 VOLTS MEAN REMOVED- .00000 VOLTS
33-1.000 CALIBRATION .00800 V/INCH
Relative
Amplitude
100 sec
Time

0000 CHANEL 1 START 0- 0- 0- 0- 0.
FILTER 2 ACF OF 100-50 MULTIPATH SIGNAL
MAX- .01200 VOLTS MEAN REMOVED- .00000 VOLTS
SR-1.000 CALIBRATION .00300 V/INCH

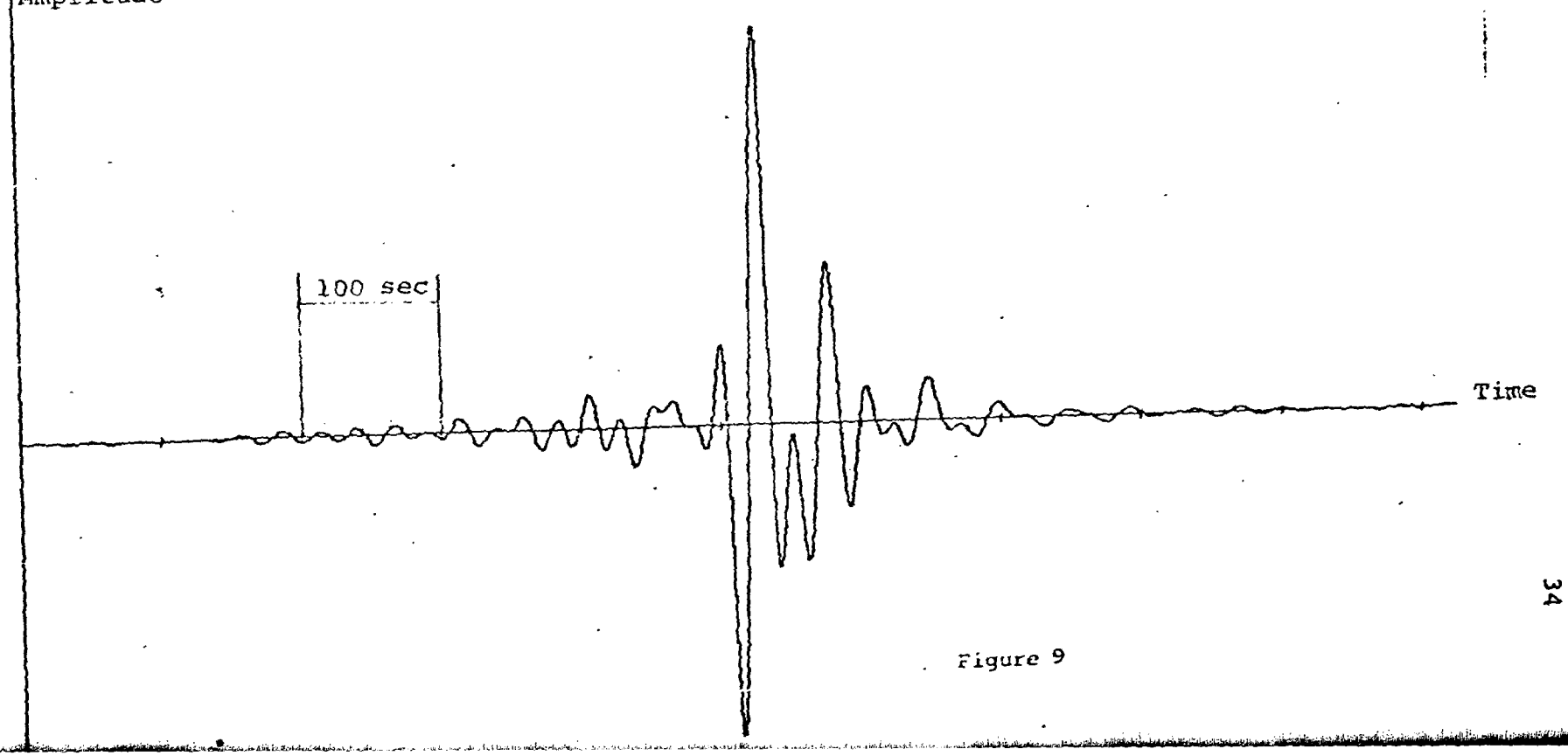

Figure 9

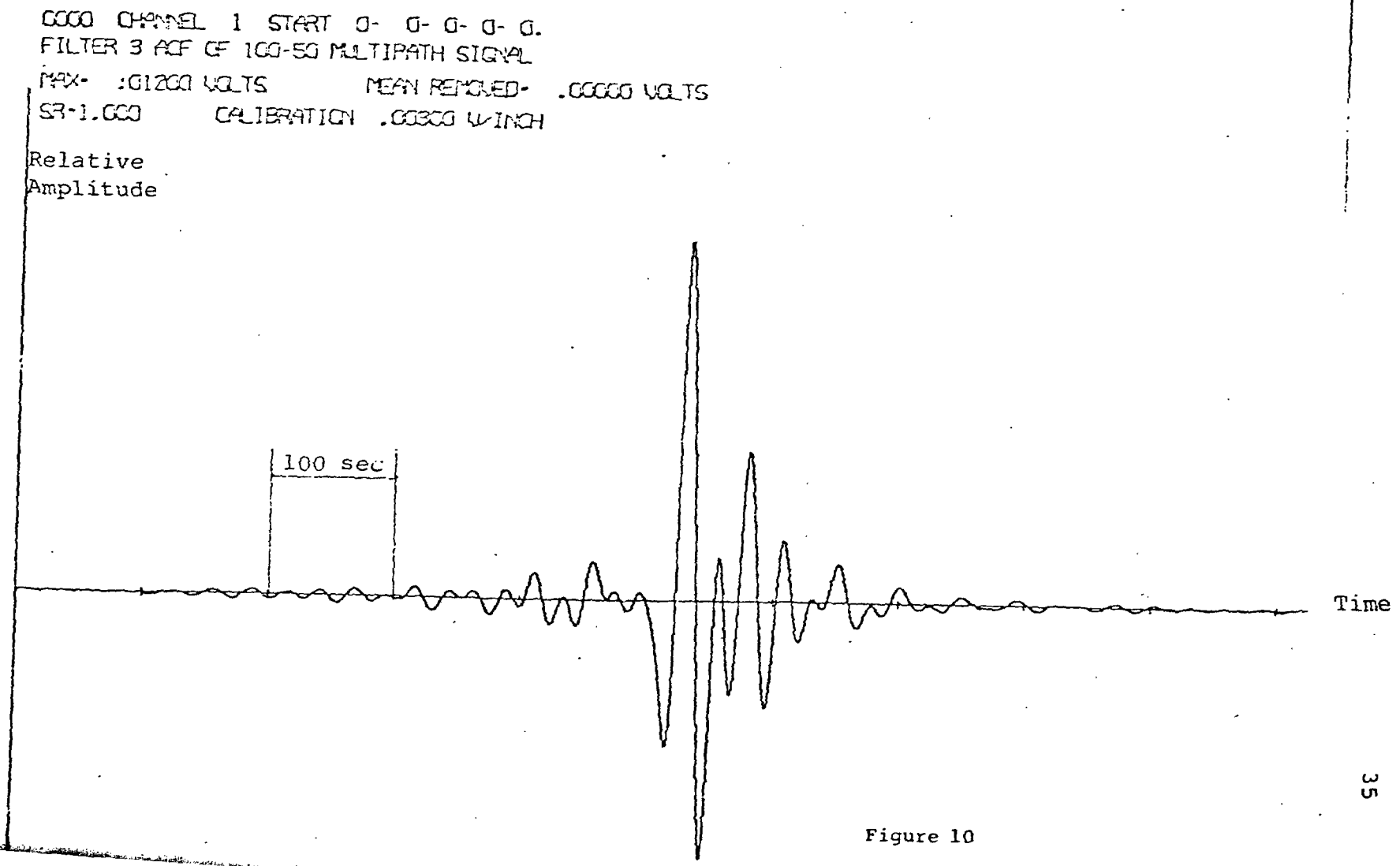
0000 CHANNEL 1 START 0- 0- 0- 0- 0.
FILTER 3 ACF OF 100-50 MULTIPATH SIGNAL
MAX- :01200 VOLTS MEAN REMOVED- .00000 VOLTS
SR-1.000 CALIBRATION .00300 V/INCH
Relative
Amplitude
100 sec
Time

Figure 10

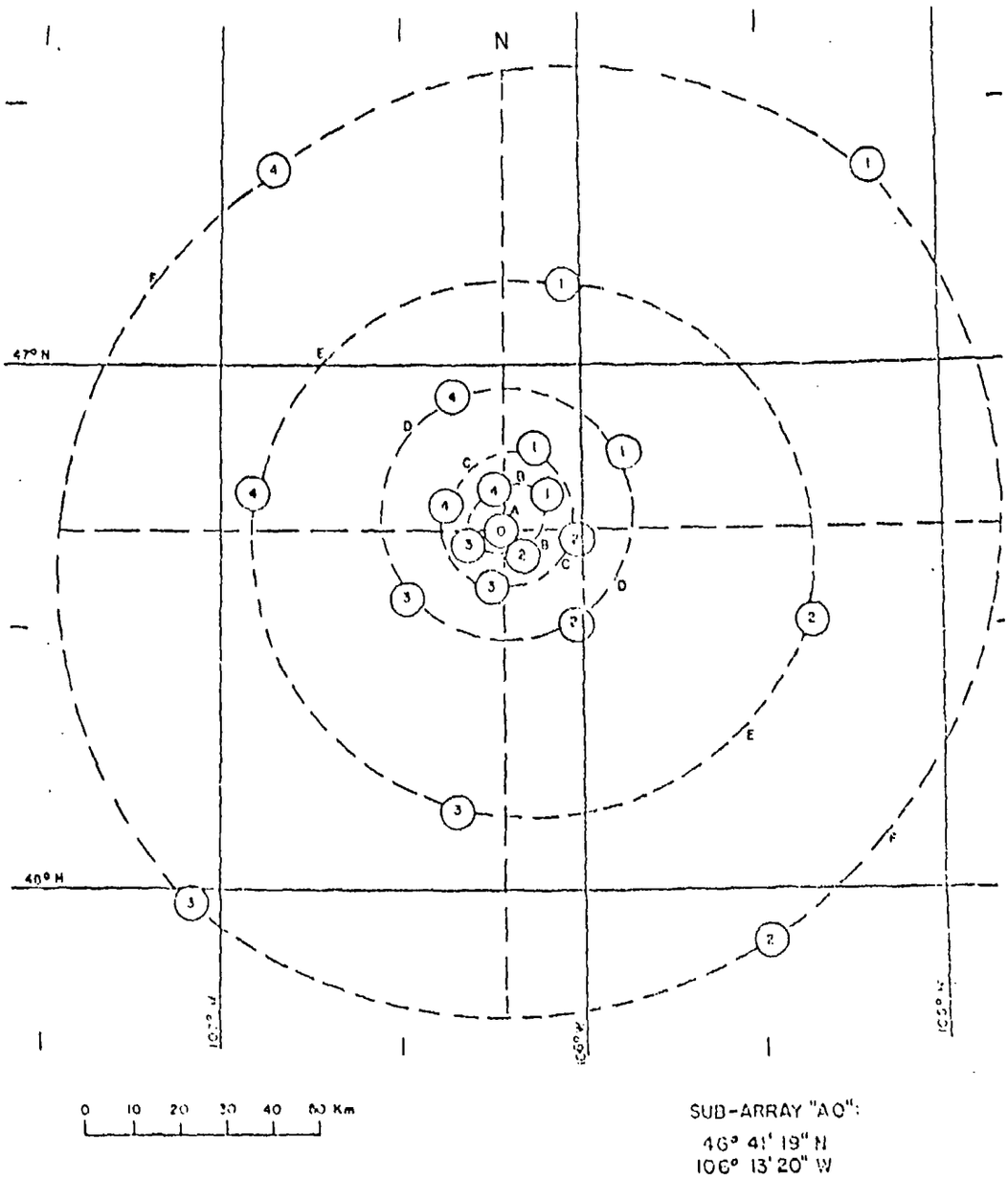

Figure 11. Configuration of the Large Aperture Seismic Array in Montana

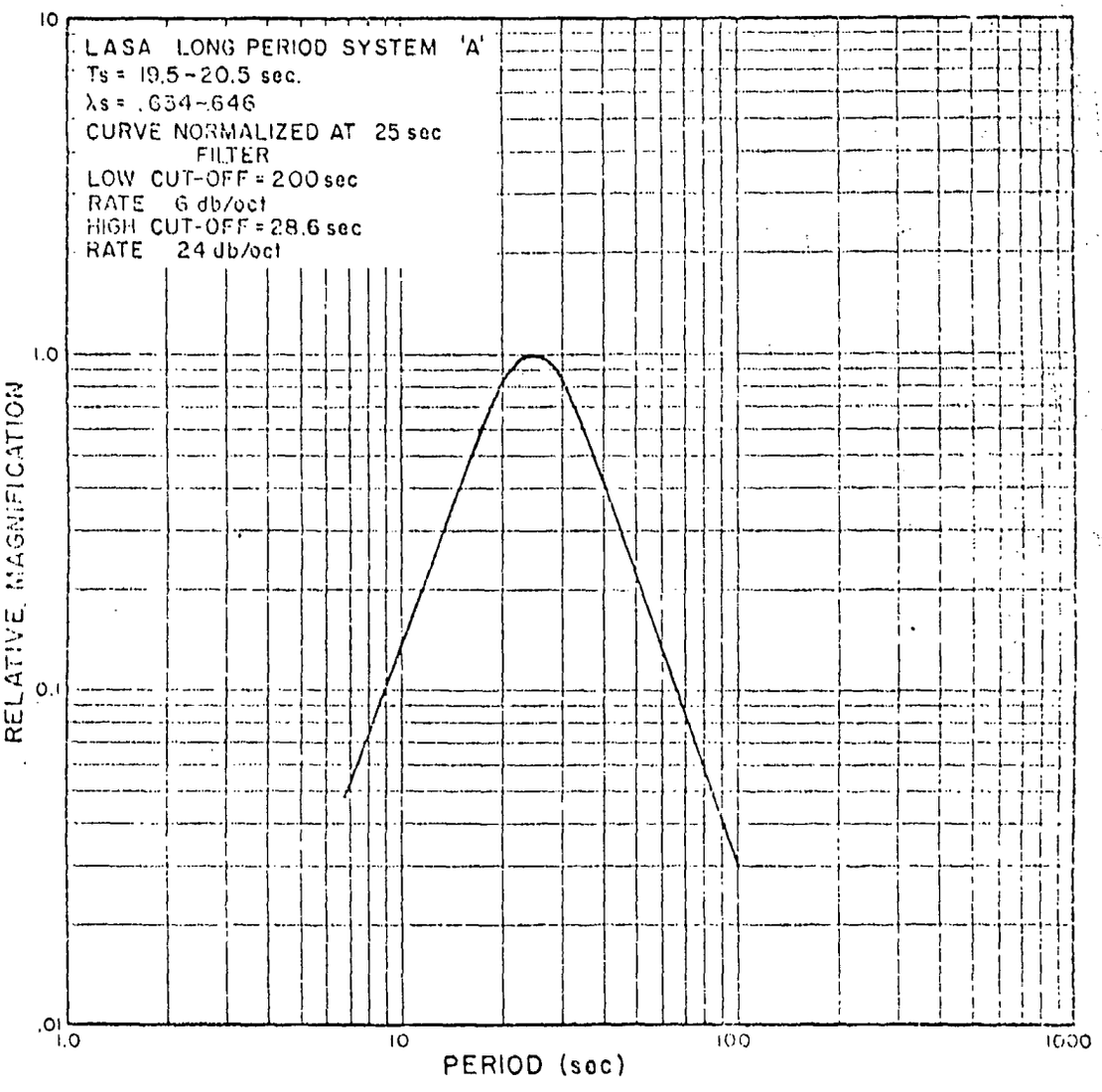

Figure 12. LASA Long Period System "A" Response

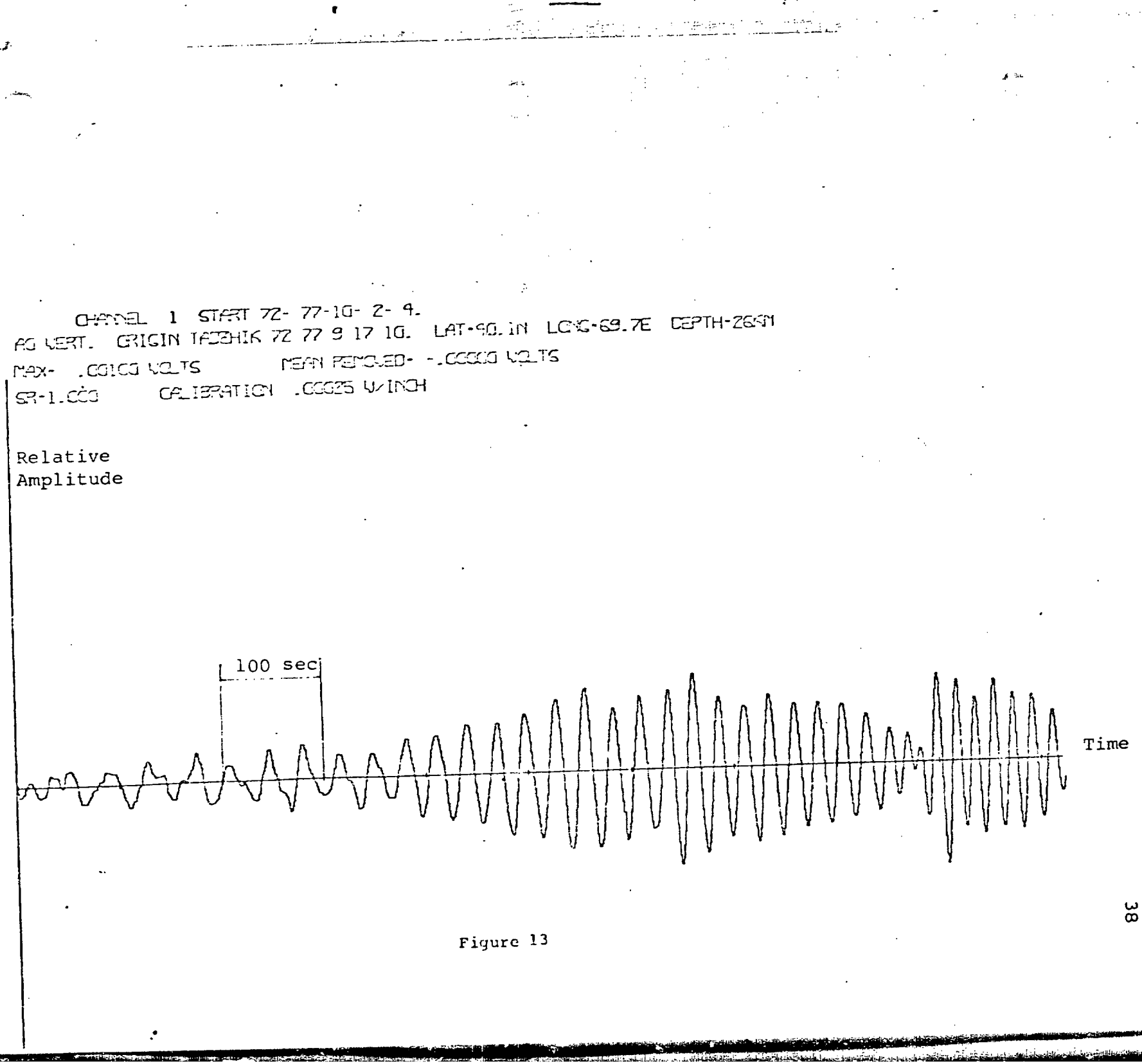
CHANNEL 1 START 72- 77-10- 2- 9.
AG VERT. ORIGIN TAZEHIK 72 77 9 17 10. LAT-90.1N LONG-69.7E DEPTH-26KM
MAX- .CC1CC VOLTS MEAN REMOVED- -.CCCCC VOLTS
SR-1.CCC CALIBRATION .CCC25 V/INCH
Relative
Amplitude
100 sec
Time

Figure 13

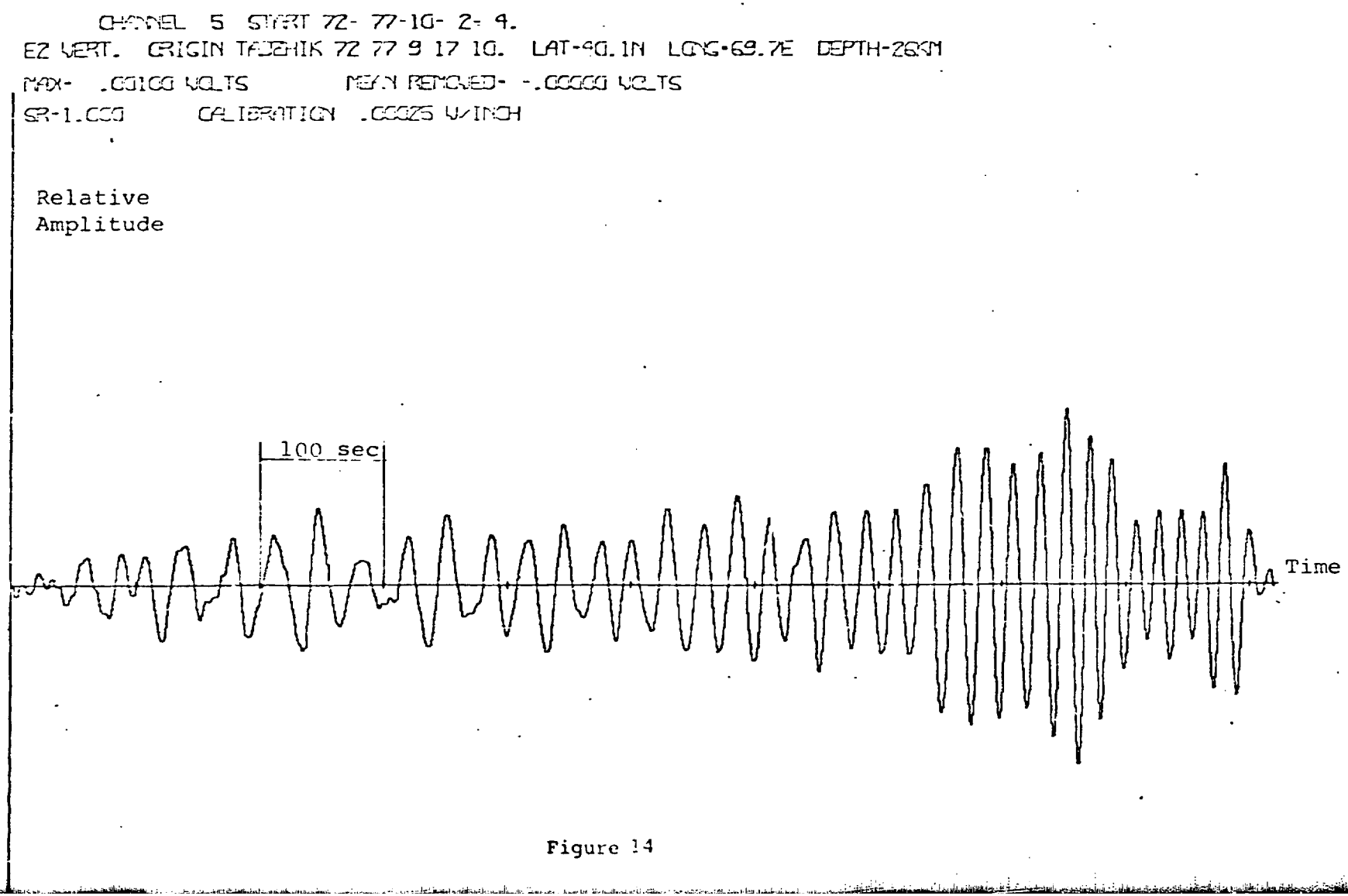
CHANNEL 5 START 72- 77-10- 2- 9.
EZ VERT. ORIGIN TAJIKH 72 77 9 17 10. LAT-40.1N LONG-69.7E DEPTH-26KM
MAX- .03100 VOLTS MEAN REMOVED- -.00000 VOLTS
SR-1.000 CALIBRATION .00025 V/INCH
Relative
Amplitude
100 sec
Time

Figure 14

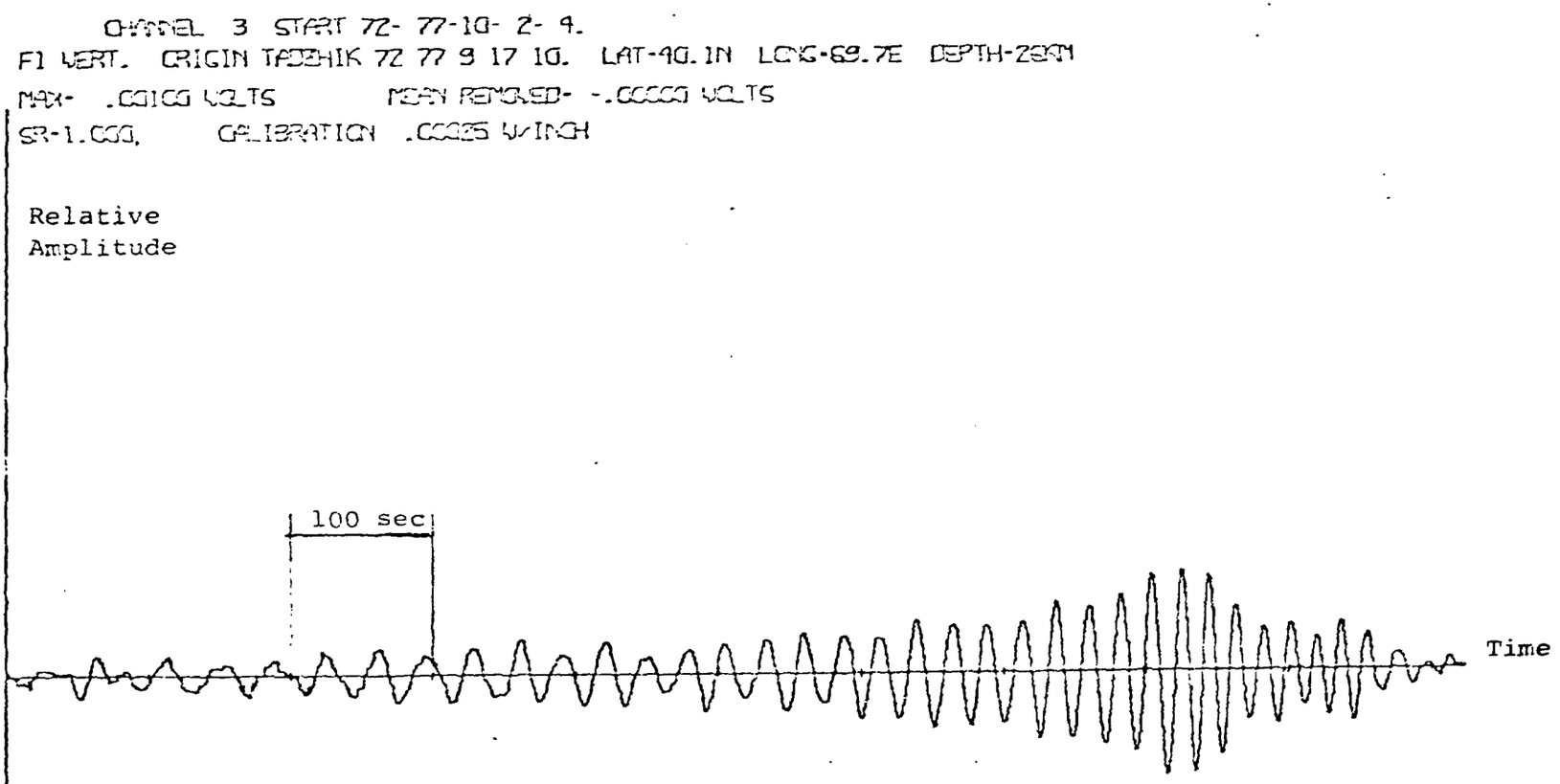
CHANNEL 3 START 72- 77-10- 2- 4.
F1 VERT. ORIGIN TADZHIK 72 77 9 17 10. LAT-40.1N LONG-69.7E DEPTH-25KM
MAX- .00106 VOLTS MEAN REMOVED- -.00000 VOLTS
SR-1.000, CALIBRATION .00025 V/INCH
Relative
Amplitude
100 sec
Time

Figure 15

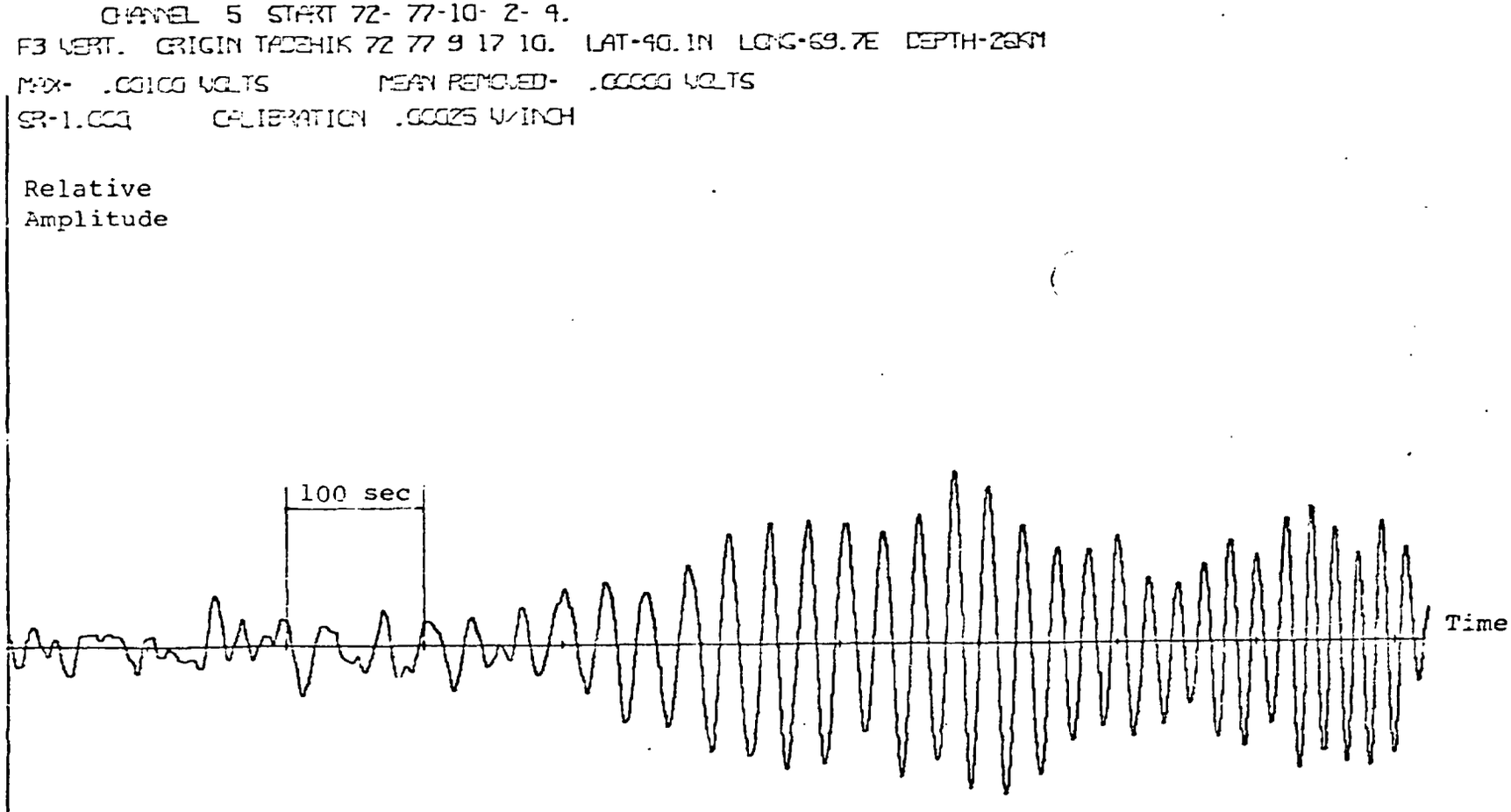
CHANNEL 5 START 72- 77-10- 2- 9.
F3 VERT. ORIGIN TADZHIK 72 77 9 17 10. LAT-40.1N LONG-69.7E DEPTH-28KM
MAX- .0010 VOLTS MEAN REMOVED- .00000 VOLTS
SR-1.000 CALIBRATION .00025 V/INCH
Relative
Amplitude
100 sec
Time

Figure 16

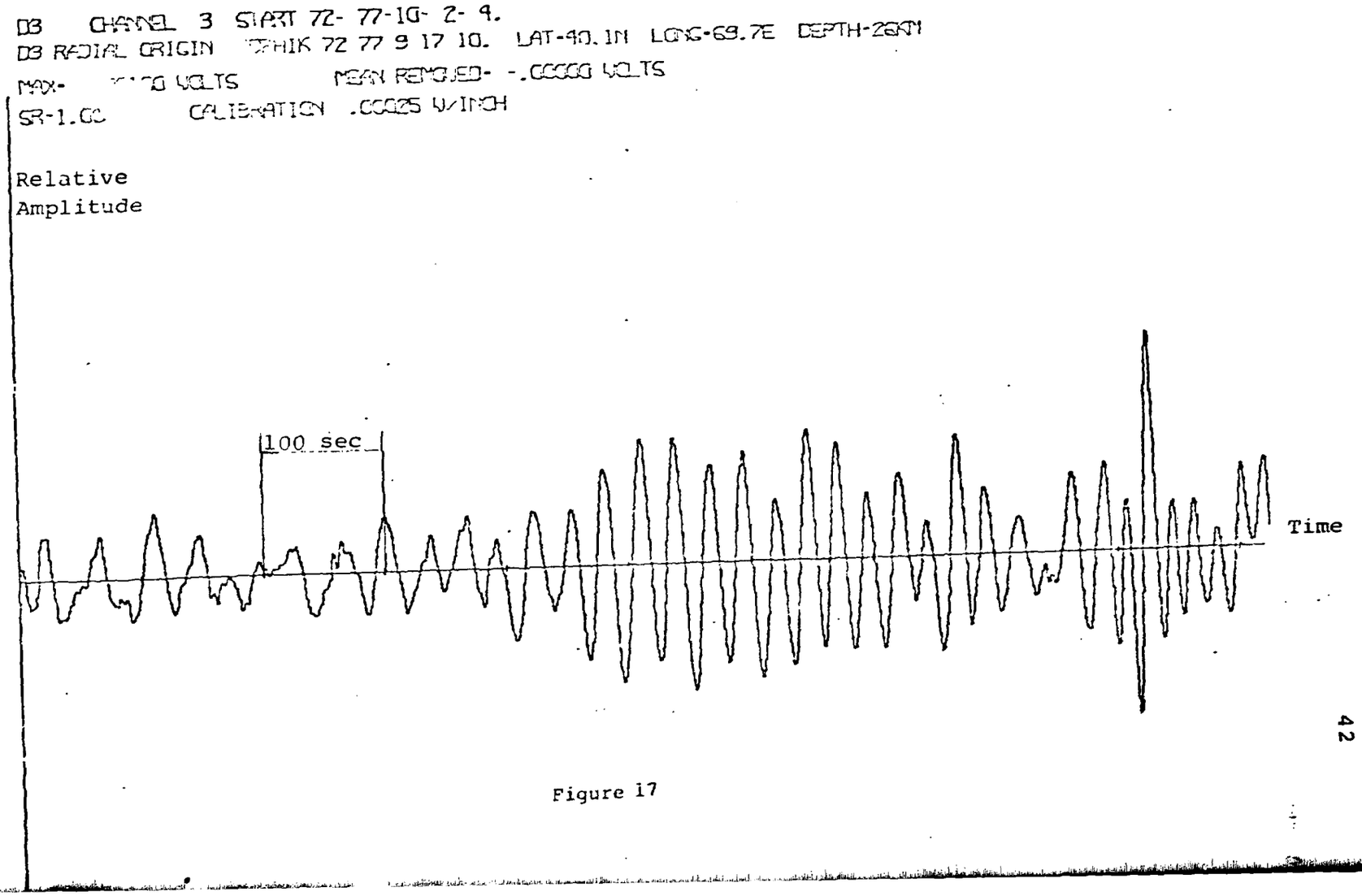
DB CHANNEL 3 START 72- 77-10- 2- 9.
DB RADIAL ORIGIN THIK 72 77 9 17 10. LAT-40.1N LONG-69.7E DEPTH-2KM
MAX- VOLTS MEAN REMOVED- -.00000 VOLTS
SR-1.00 CALIBRATION .00025 V/INCH
Relative
Amplitude
100 sec
Time

Figure 17

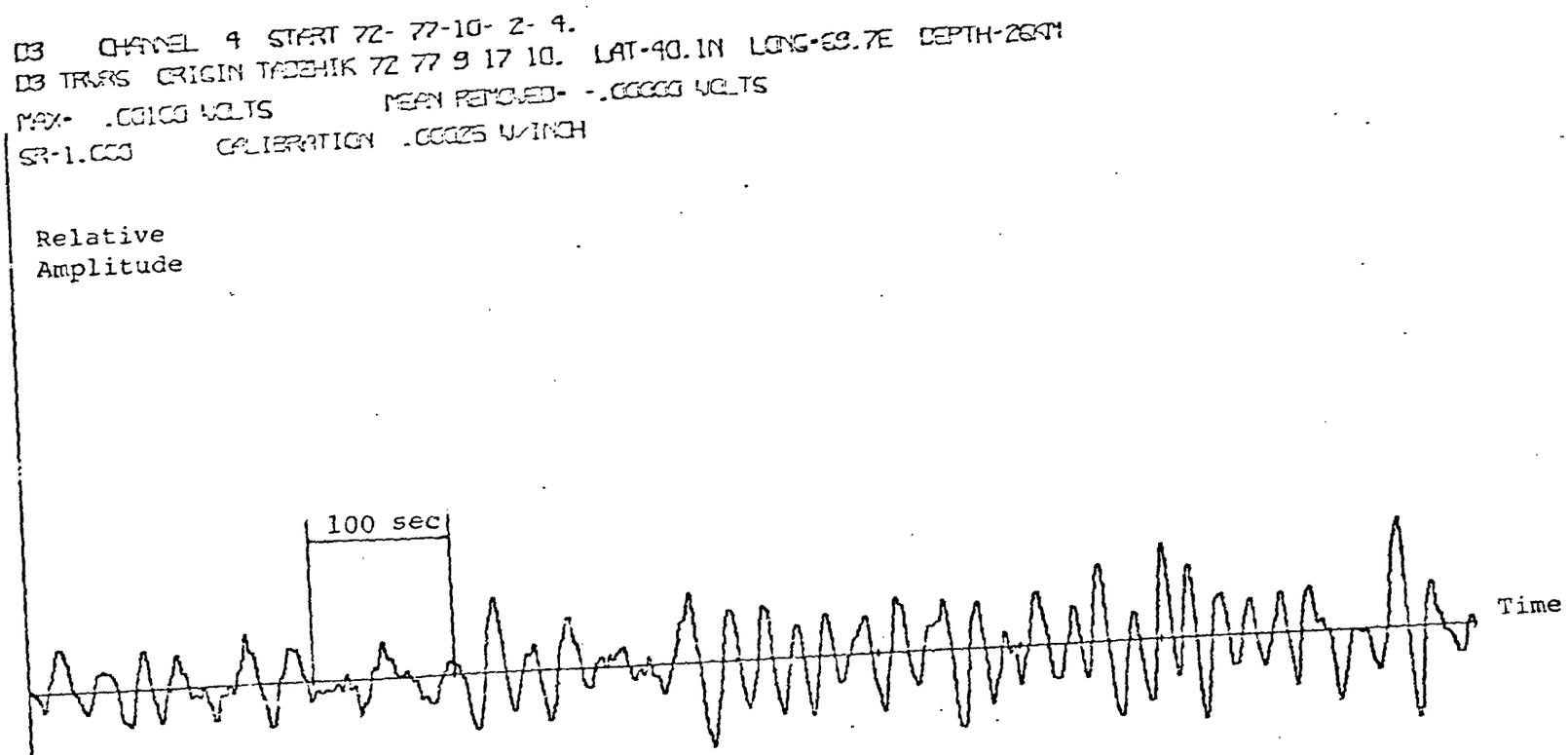
D3 CHANNEL 4 START 72- 77-10- 2- 4.
D3 TRANS ORIGIN TADZHIK 72 77 9 17 10. LAT-40.1N LONG-69.7E DEPTH-26KM
MAX- .C01CC VOLTS MEAN REMOVED- -.CCCCC VOLTS
SR-1.CCC CALIBRATION .CCC25 V/INCH
Relative
Amplitude
100 sec
Time

Figure 18

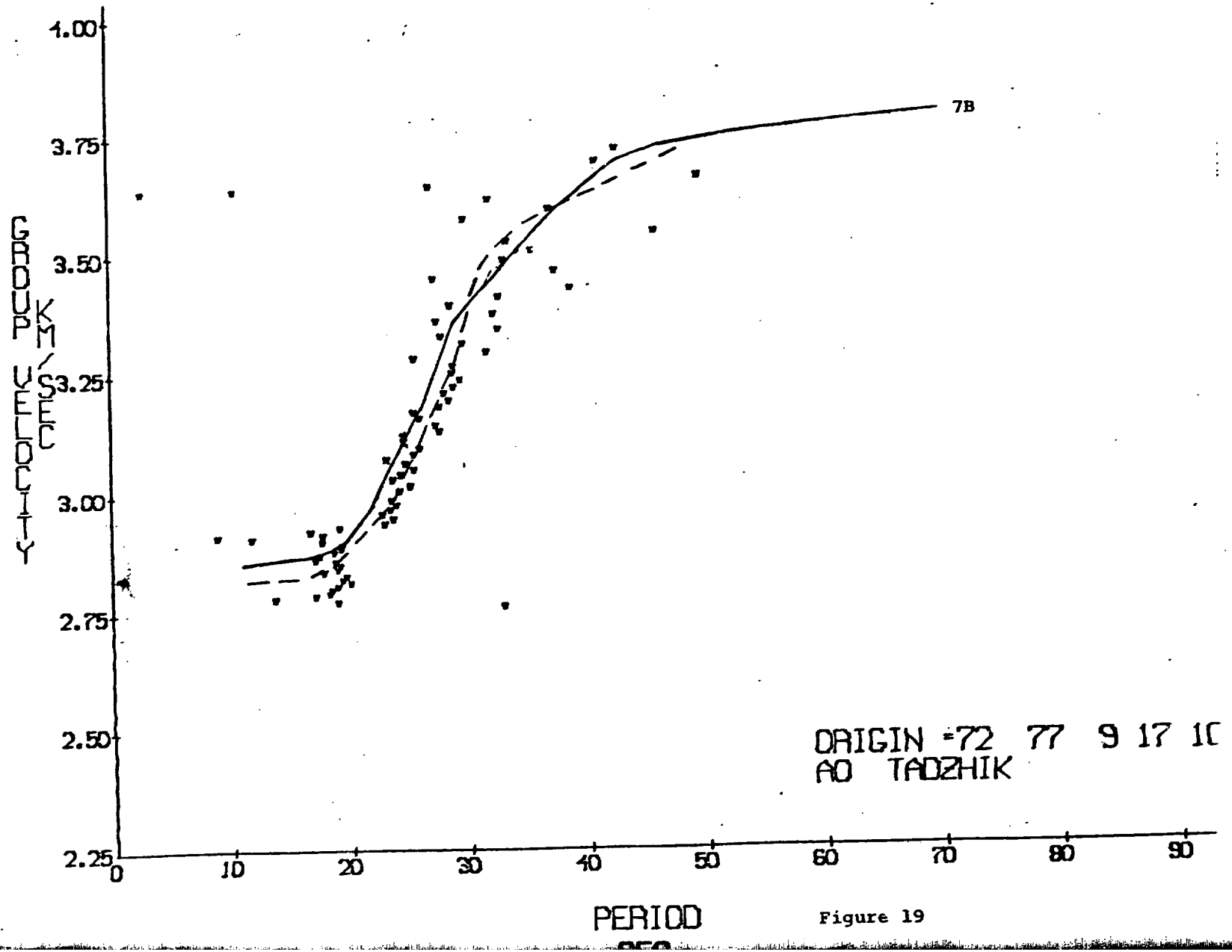
4.00
3.75
3.50
3.25
3.00
2.75
2.50
2.25
GROUP VELOCITY KM/SEC
0
10
20
30
40
50
60
70
80
90
PERIOD
7B
ORIGIN =72 77 9 17 1C
AO TADZHIK

Figure 19

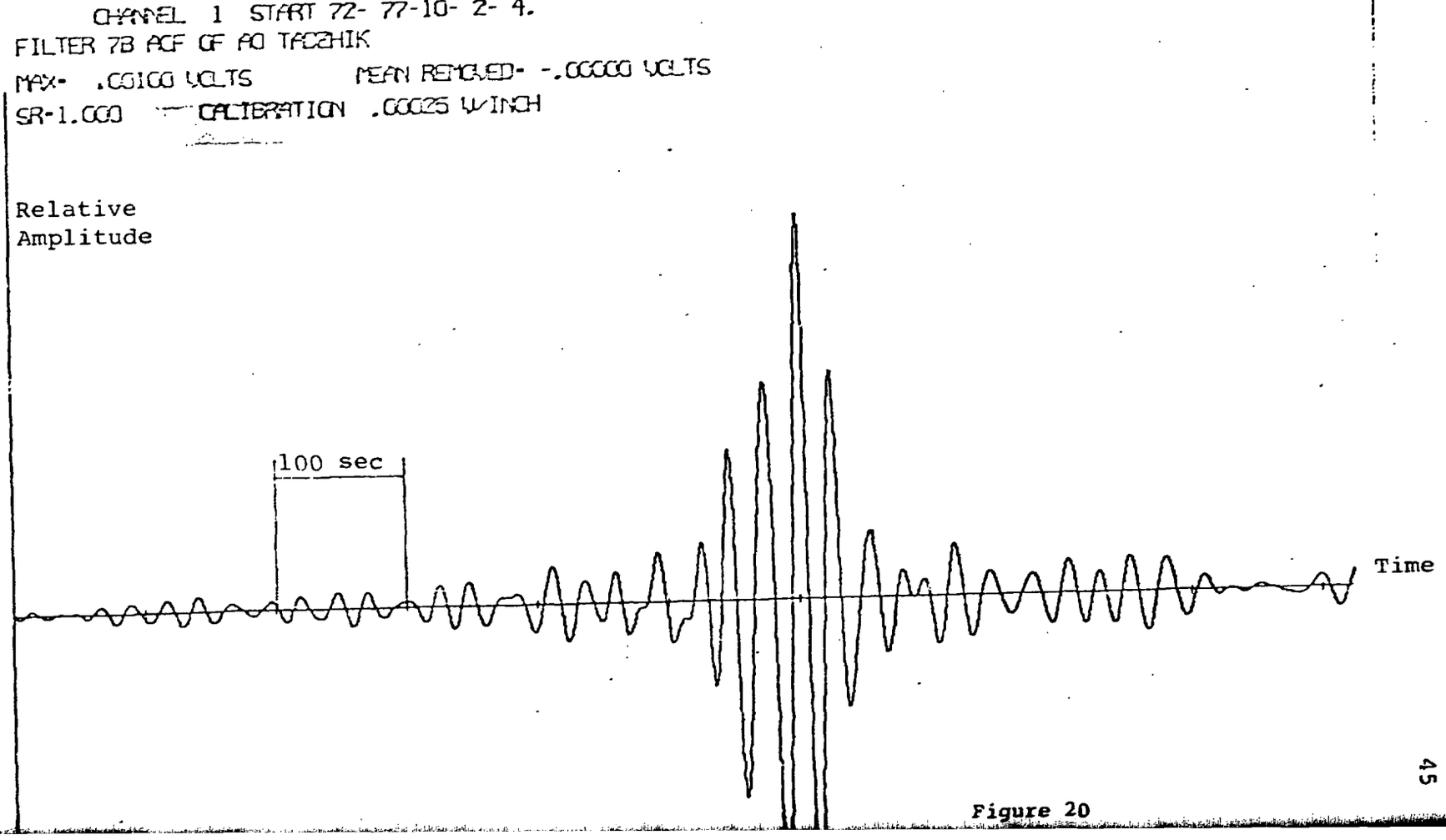
CHANNEL 1 START 72- 77-10- 2- 4.
FILTER 7B ACF OF AO TAOZHIK
MAX- .CS1CO VOLTS MEAN REMOVED- -.OOOOO VOLTS
SR-1.OOO CALIBRATION .OOO25 V/INCH
Relative
Amplitude
100 sec
Time

Figure 20

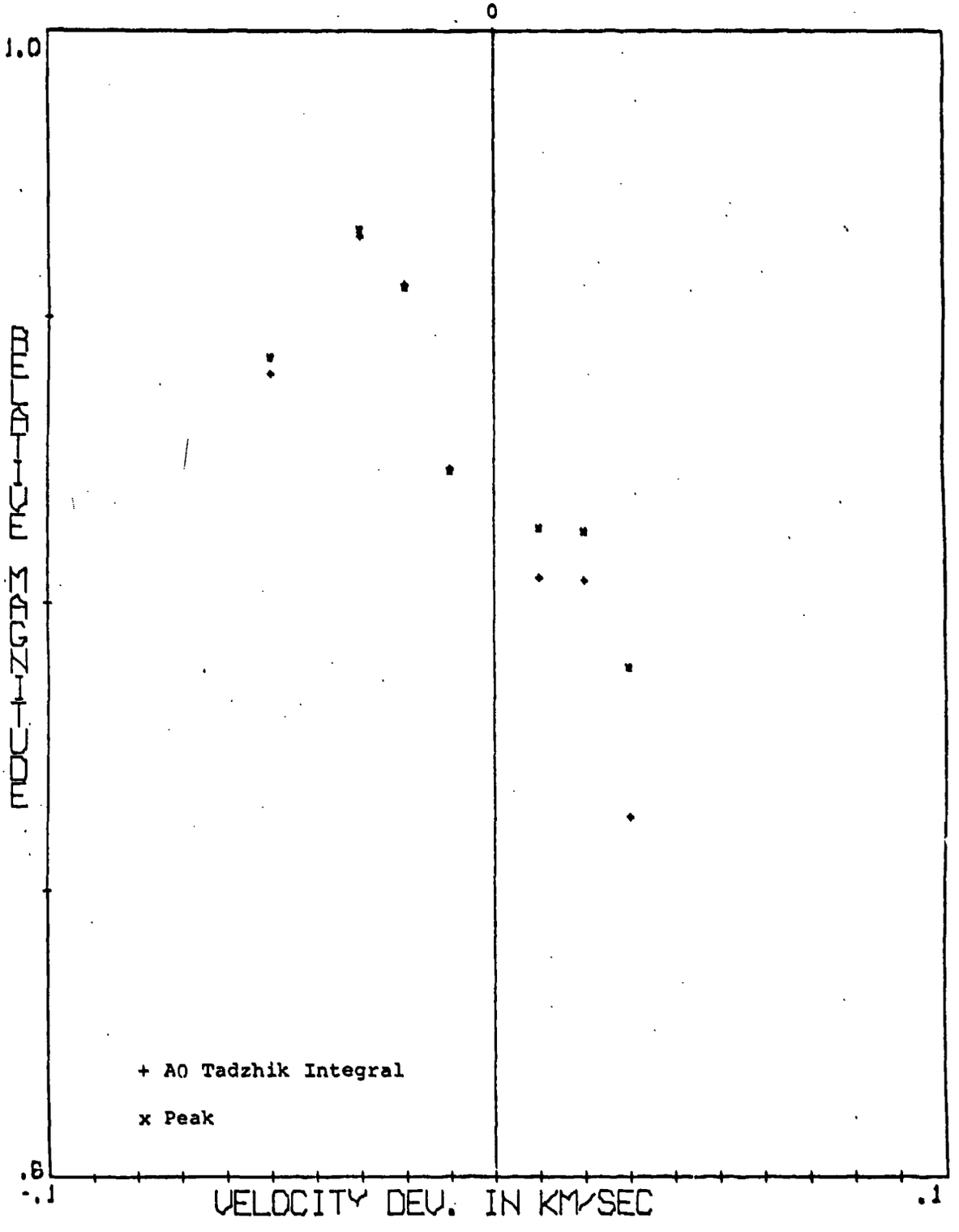
0
1.0
.6
-.1
.1
RELATIVE MAGNITUDE
VELOCITY DEV. IN KM/SEC
+ A0 Tadzhik Integral
x Peak

Figure 21

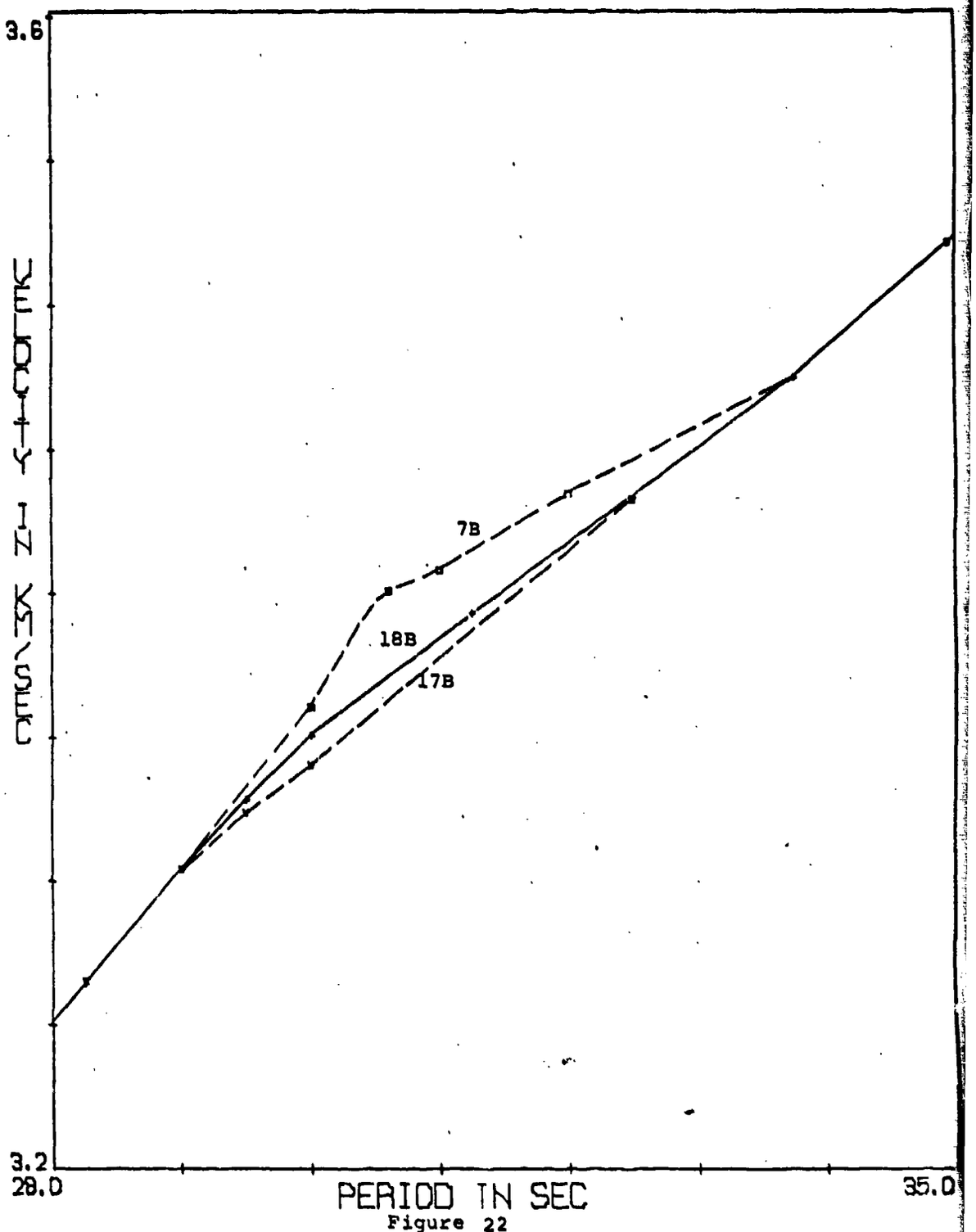

Figure 22

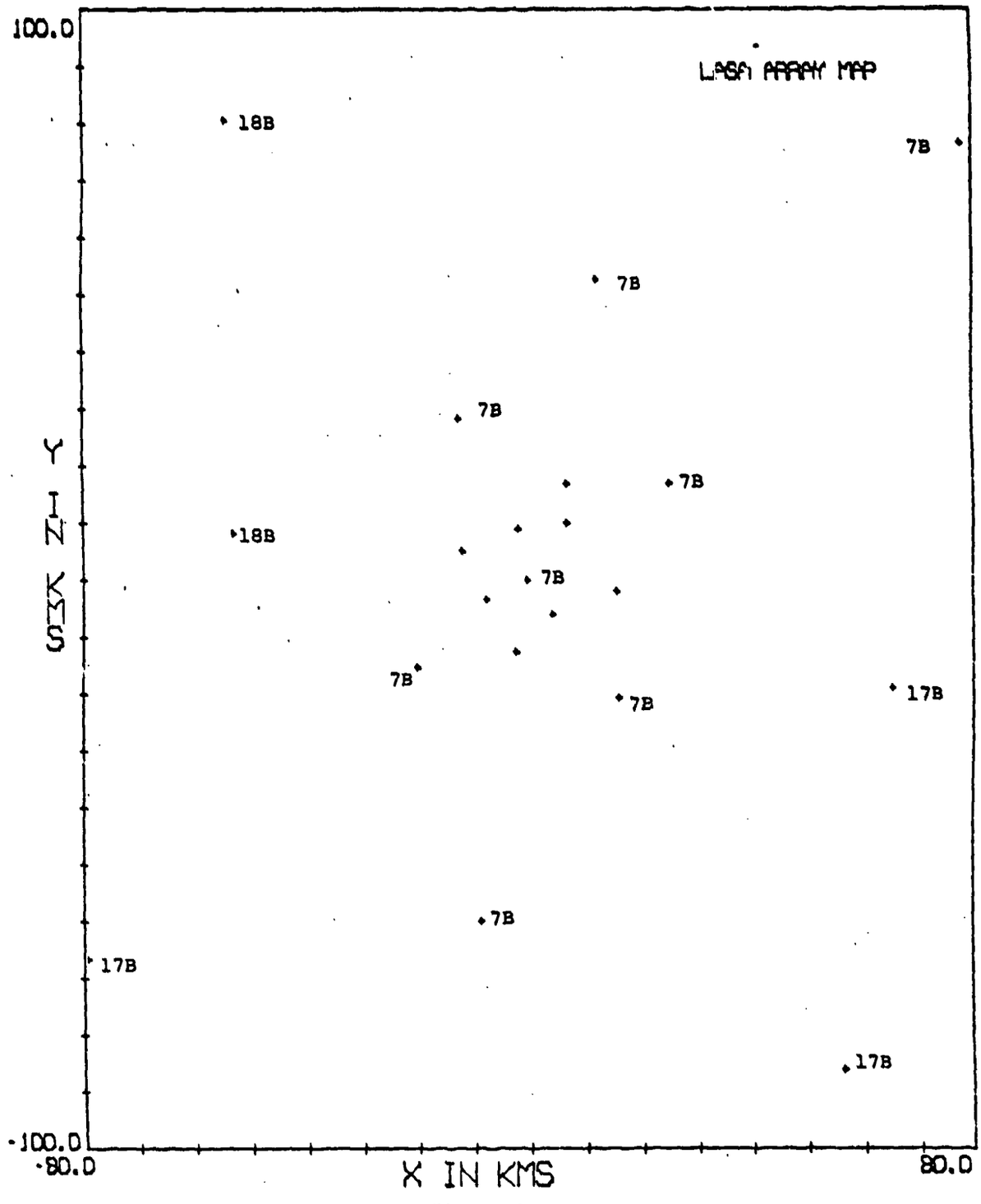

Figure 23

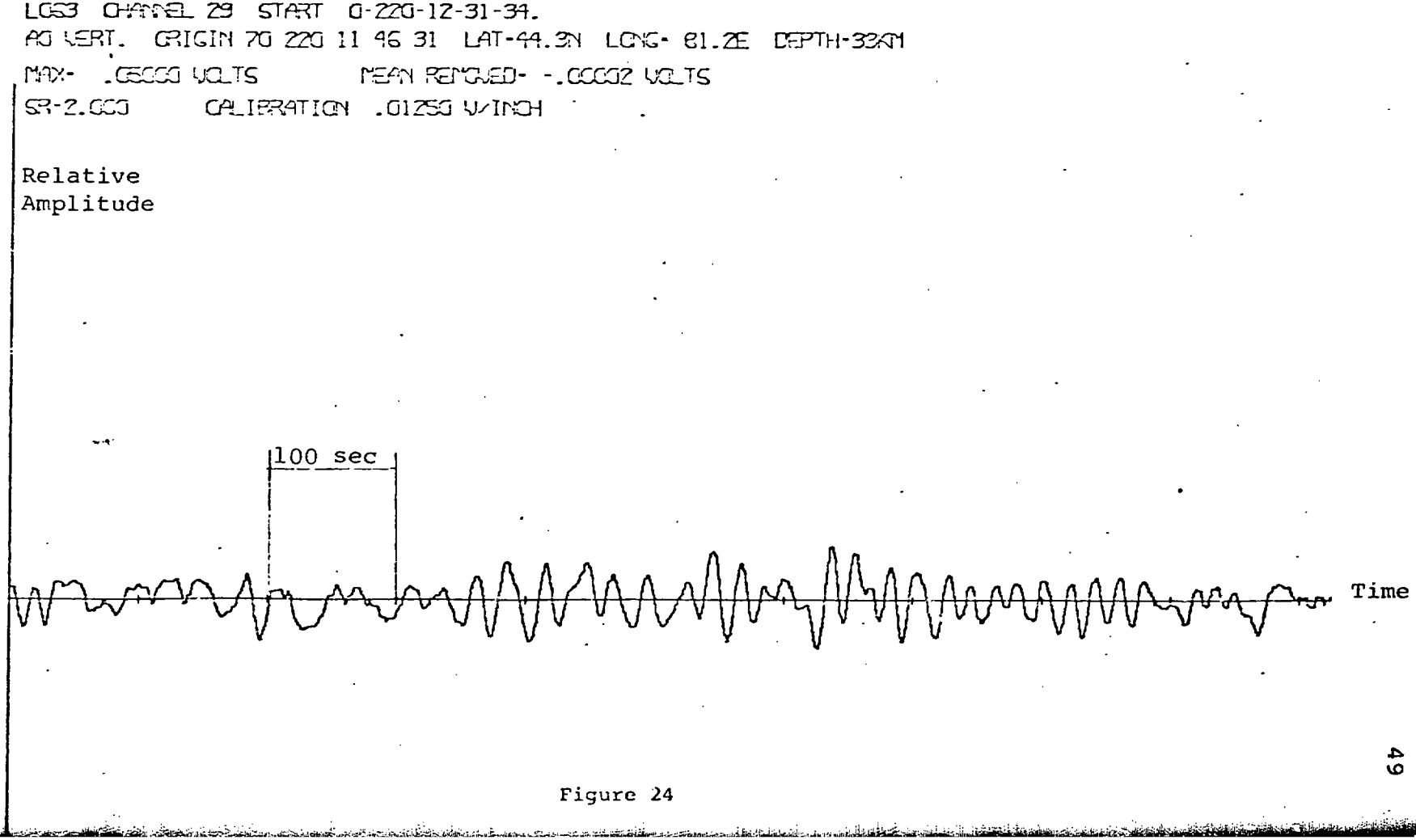
LGSB CHANNEL 29 START 0-220-12-31-34.
AO VERT. ORIGIN 70 220 11 46 31 LAT-44.3N LONG- 81.2E DEPTH-33KM
MAX- .05000 VOLTS MEAN REMOVED- -.00002 VOLTS
SR-2.000 CALIBRATION .01250 V/INCH
Relative
Amplitude
100 sec
Time

Figure 24

LG63 CHANNEL 29 START 0-220-12-31-39.
.183 PCF ORIGIN 70 220 11 46 31 LAT-44.3N LONG- 81.2E DEPTH-33KM
MAX- .05000 VOLTS MEAN REMOVED- -.00001 VOLTS
SR-2.000 CALIBRATION .01250 V/INCH

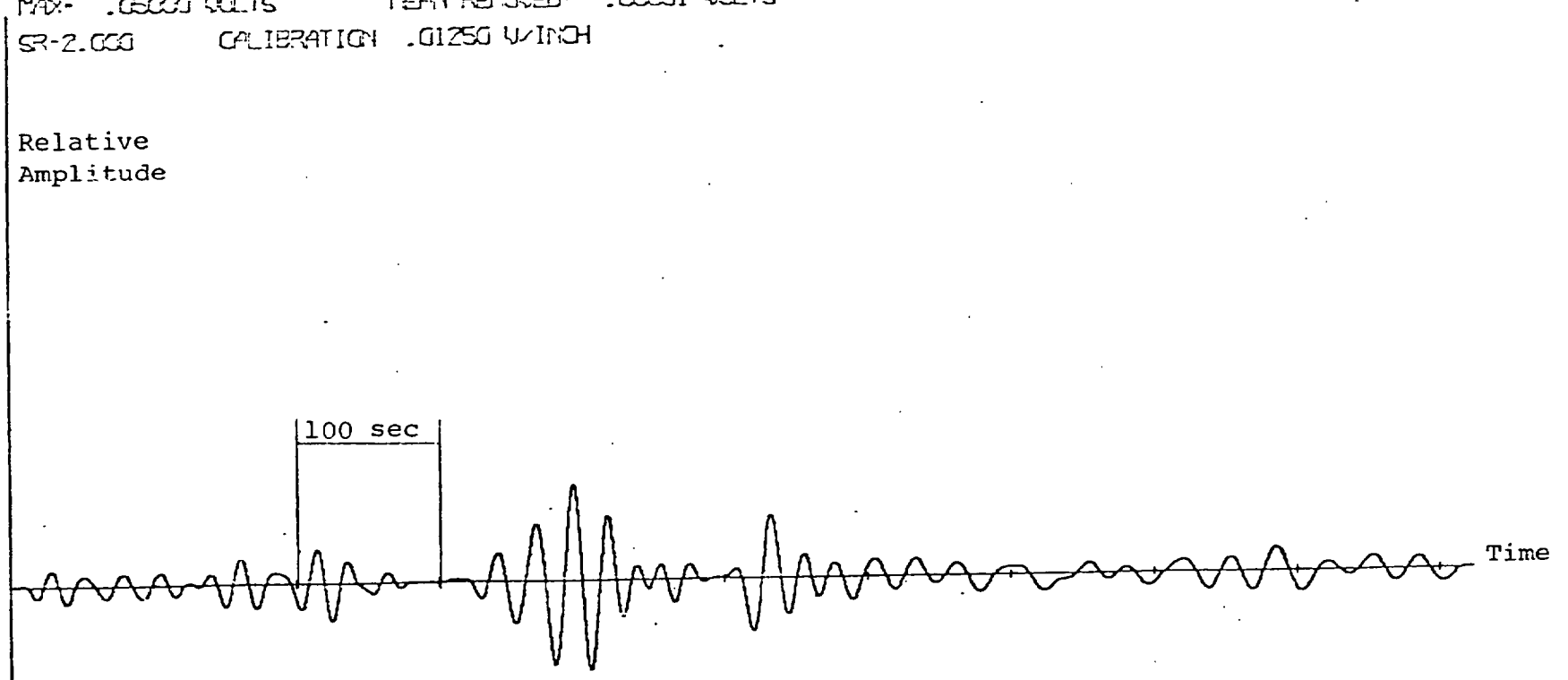

Figure 25

REFERENCES

Bloch, S. and A. L. Hales, New techniques for the determination of surface wave phase velocities, Bull. Seis. Soc. Am., 58, p. 1021-1034, 1969.

Bracewell, R. M., The Fourier Transform and its Applications, McGraw-Hill, Inc., 1965.

Bullen, K. E., An Introduction to the Theory of Seismology, 3rd ed., Cambridge Univ. Press, 1963.

Capon, J., R. J. Greenfield, and R. T. Lacoss, Long period signal processing results for the large aperture seismic array, Geoph., 34, p. 305-329, 1968.

Dziewonski, A., S. Bloch, and M. Landisman, A technique for the analysis of transient seismic signals, Bull. Seis. Soc. Am., 59, p. 427-444, 1969.

Ewing, M. and F. Press, Crustal structure and surface wave dispersion, part 2, Bull. Seis. Soc. Am., 42, p. 315-325, 1952.

Filon, L. N. G., On a quadrature formula for trigonometric integrals, Proc. Roy. Soc. Edin., 49, p. 38-47, 1929.

Kanasewich, E. R., Time Sequence Analysis in Geophysics, Univ. Alberta Press, 1973.

Landisman, M., A. Dziewonski and Y. Sato, Recent improvements in the analysis of surface wave observations, Geophy. J. R. Astr. Soc., 17, p. 369-403, 1969.

McDonald, J. A., W. Tucker, and E. Herrin, Matched filter detection of surface waves of periods up to seventy-five seconds generated by small earthquakes, Bull. Seis. Soc. Am., 64, p. 1843-1854, 1974.

Nyman, D. C. and M. Landisman, Improvements in frequency-time analysis and time variable filters, submitted to Geoph. J. R. Astr. Soc., 14 p., 1975.

Oliver, J., A summary of observed seismic surface wave dispersion, Bull. Seis. Soc. Am., 52, p. 81-85, 1962.

Sato, Y., Analysis of dispersed surface waves by means of Fourier Transform 1, Bull. Earthquake Res. Inst., Tokyo Univ., Part 1, 33, p. 33-47, 1955.

Sutton, D. J., Rayleigh wave group velocities in central California, Bull. Seis. Soc. Am., 58, p. 881-890, 1968.

Wainstein, L. A. and V. D. Zubakov, Extraction of Signals from Noise, Prentice Hall, Inc., 1962.